

IR nebulae around bright massive stars as indicators for binary interactions

J. Bodensteiner^{1,2,3}, D. Baade⁴, J. Greiner³, and N. Langer⁵

¹ Instituut voor Sterrenkunde, KU Leuven, Celestijnenlaan 200D, Bus 2401, 3001 Leuven, Belgium
e-mail: julia.bodensteiner@kuleuven.be

² Technische Universität München, James-Franck-Straße 1, 85748 Garching, Germany

³ Max-Planck-Institut für extraterrestrische Physik, Gießenbachstraße, 85748 Garching, Germany

⁴ European Southern Observatory, Karl-Schwarzschild-Straße 2, 85748 Garching, Germany

⁵ Argelander-Institut für Astronomie der Universität Bonn, Auf dem Hügel 71, 53121 Bonn, Germany

Received Month xx, xxxx; accepted Month xx, xxxx

ABSTRACT

Context. Recent studies show that more than 70% of massive stars do not evolve as effectively single stars, but as members of interacting binary systems. The evolution of these stars is thus strongly altered compared to similar but isolated objects.

Aims. We investigate the occurrence of parsec-scale mid-infrared nebulae around early-type stars. If they exist over a wide range of stellar properties, one possible overarching explanation is non-conservative mass transfer in binary interactions, or stellar mergers.

Methods. For ~ 3850 stars (all OBA stars in the Bright Star Catalogue [BSC], Be stars, BeXRBs, and Be+sdO systems), we visually inspect WISE $22\mu\text{m}$ images. Based on nebular shape and relative position, we distinguish five categories: offset bow shocks structurally aligned with the stellar space velocity, unaligned offset bow shocks, and centered, unresolved, and not classified nebulae.

Results. In the BSC, we find that 28%, 13%, and 0.4% of all O, B, and A stars, respectively, possess associated infrared (IR) nebulae. Additionally, 34/234 Be stars, 4/72 BeXRBs, and 3/17 Be+sdO systems are associated with IR nebulae.

Conclusions. Aligned or unaligned bow shocks result from high relative velocities between star and interstellar medium (ISM) that are dominated by the star or the ISM, respectively. About 13% of the centered nebulae could be bow shocks seen head- or tail-on. For the rest, the data disfavor explanations as remains of parental disks, supernova remnants of a previous companion, and dust production in stellar winds. The existence of centered nebulae also at high Galactic latitudes strongly limits the global risk of coincidental alignments with condensations in the ISM. Mass loss during binary evolution seems a viable mechanism for the formation of at least some of these nebulae. In total, about 29% of the IR nebulae (2% of all OBA stars in the BSC) may find their explanation in the context of binary evolution.

Key words. – stars: early-type; emission-line, Be; rotation – binaries – circumstellar matter – ISM: dust

1. Introduction

Recent observations indicate that about 70% of all O stars are members of interacting binary systems and undergo mass transfer phases at some point of their evolution (Sana et al. 2012). Close binary interactions thus strongly influence the evolution of a large number of massive stars (Podsiadlowski et al. 1992; Wellstein & Langer 1999; de Mink et al. 2014). Different interaction channels are possible, consisting of tidal interactions (Zahn 1975; de Mink et al. 2009), mass and angular momentum transfer via Roche lobe overflow (RLOF, Paczynski 1981; Shu & Lubow 1981), common-envelope (CE) phase (Paczynski 1976; Iben & Livio 1993), and stellar merger (Podsiadlowski et al. 1992; Wellstein et al. 2001; Tylenda et al. 2011).

The outcome of such binary interactions depends strongly on the initial mass ratio and the orbital separation of the system (de Mink et al. 2013). In wider systems, the mass transfer typically occurs when the donor expands after leaving the main sequence (MS, de Mink et al. 2013), commonly referred to as "case B mass transfer" (Kippenhahn & Weigert 1967). When mass is transferred during a sufficiently stable RLOF phase, the companion accretes the material and angular momentum and is spun up efficiently. In conservative mass transfer, the companion is able to accrete all material transferred from the primary, while in the

non-conservative case, material is lost to the surroundings because the companion cannot accrete at the same rate (Petrovic et al. 2005; Tout 2012).

After the main mass transfer event in a binary, which could be a RLOF or a CE evolution, the mass donor will evolve through a phase as helium star before reaching its end stage. This is best confirmed in the low-mass regime by the so-called subdwarfs. Subdwarfs are (mostly) helium-core burning stars that have almost completely lost their hydrogen envelope and have a narrow mass distribution centered on $0.47 M_{\odot}$. Subdwarfs are mainly divided into two groups, sdOs and sdBs, depending on their temperature, which can reach more than 50 000 K (Heber 2009, 2016).

In the intermediate- and high-mass regime, helium stars are expected to reach temperatures of up to 100 000 K (Yoon et al. 2010; Langer 2012; Gotberg et al. 2017), which renders their direct detection difficult, such that only a few counterparts are known (Schootemeijer et al. 2018). However, strong evidence for their existence comes from the Be-X-ray binaries, which require an intermediate-mass helium star as neutron star progenitor (van den Heuvel & Rappaport 1987). For the most massive progenitors, the helium stars obtain strong winds and are easily identified as Wolf-Rayet stars with strong emission lines, such

that the helium-star stage of binary evolution is again observationally well confirmed (Petrovic et al. 2005).

Depending on the initial masses of the two components, the mass donor will end up as a white dwarf (WD), a neutron star (NS), or a black hole (BH) (Portegies Zwart 1995; Han et al. 2002). WDs are difficult to detect in massive binary systems because of their low luminosity and mass. They may, however, reveal themselves if they are interacting with their companion through mass transfer. Such systems appear as so-called cataclysmic variables (Robinson 1976), Supersoft X-Ray Sources (Kahabka & van den Heuvel 1997) or symbiotic binaries (Kenyon & Webbink 1984), in which matter is accreted from the companion onto the WD via an accretion disk.

If the initial mass of the primary is sufficiently high, the interaction may result in the formation of an NS (Rappaport & van den Heuvel 1982) or even a BH (Zhang et al. 2003; Casares et al. 2014). Because material is also accreted onto the compact object, these systems are strong X-ray sources, known as X-ray binaries (XRBs). They can be detected out to large distances because of this strong but transient X-ray emission (Haberl & Sasaki 2000; Reig 2011). When forming an NS, the primary is disrupted in a supernova (SN) explosion. The sudden mass loss caused by the ejection of the exploding star's envelope drastically changes the binary parameters and can lead to the breakup of the system. For a circular orbit, and if the NS birth kick is neglected, the system remains bound if the ejected mass is lower than half the total system mass (Blaauw 1961). Owing to asymmetries in the supernova, a kick can be induced in a random direction that might hinder or support the breakup of the system (Martin et al. 2009).

Massive stars in close binary systems with similar initial masses and short periods may even merge, forming a fast-rotating single star (Podsiadlowski et al. 1992). In addition to the fast rotation, the product of a stellar merger may show higher abundances of processed material (e.g., nitrogen), and appears rejuvenated compared to other stars in the same stellar population (Glebbeek et al. 2013). During the merging process, the huge excess of angular momentum can lead to the ejection of mass (between 2 – 8% of the total mass of the system), depending on the initial mass ratio and the evolutionary status of the stars (Glebbeek et al. 2013). In mergers of massive stars, a few solar masses might be lost, which would lead to the formation of a massive circumstellar nebula (Schneider et al. 2016). The material in such nebulae dissipates on timescales shorter than 10 000 yr (Schneider et al. 2016), limiting their observability.

Systems with extreme mass ratios evolve into a CE phase directly after the onset of mass transfer (de Mink et al. 2013), in which both stars orbit each other inside a single, shared envelope (Ivanova et al. 2013). CE phases are thought to be too short to lead to a substantial spin-up of the companion (de Mink et al. 2013; Shao & Li 2014). However, both RLOF (Packet 1981) and stellar mergers (Podsiadlowski et al. 1992) can result in the formation of fast-rotating stars as the angular momentum transfer spins up the companion star significantly (Sills et al. 2005; de Mink et al. 2013).

Several authors have predicted that if the companion is a B star, such spin-up in a binary system will turn it into a Be star (Packet 1981; Rappaport & van den Heuvel 1982; Pols et al. 1991). Classical Be stars are defined as "rapidly rotating main-sequence (MS) B-type stars that are forming an outwardly diffusing gaseous, dust-free Keplerian disk" (Rivinius et al. 2013, but see also Collins 1987). The process that transports matter onto a Keplerian orbit is still unknown but probably involves the combination of near-critical rotation and nonradial pulsation

(Rivinius et al. 1998; Baade et al. 2017). In the disk, the material is governed by viscosity (Lee et al. 1991; Carciofi et al. 2009) and leads to prominent Balmer emission lines (Rivinius et al. 2013).

Binary population synthesis studies show that it cannot be excluded that most (or even all) Be stars are formed through mass exchange with or without subsequent merger (Vanbeveren & Mennekens 2017). Other possible pathways that lead to fast rotation are that the stars could be born as fast rotators (Bodenheimer 1995; Martayan et al. 2007) or spin up during MS evolution when angular momentum from the core is transferred onto the envelope (Ekström et al. 2008) and, perhaps, by nonradial g -mode pulsations. Possibly, not all Be stars are spun up by the same process, but some or all of these models play an important role (see, e.g., McSwain & Gies 2005, Huang et al. 2010). As the models are not mutually exclusive, however, a single-model-specific tracer is required to distinguish between them.

Here, we report on a search for hints of close-binary interactions by investigating the stellar surroundings at mid-IR wavelengths in different input samples of early-type stars that we visually inspect in WISE 22 μm data. On the one hand, we investigate the surroundings of three lists of peculiar subtypes of stars, that is, Be stars, BeXRBs, and Be+sdO systems. On the other hand, to place these searches in a broader context, we also inspect the surroundings of all ~ 3800 OBA stars in the Bright Star Catalogue (BSC, Hoffleit & Jaschek 1991) consisting of all stars with $V \leq 6.5$. We characterize the stars by a literature search, explore the origin and nature of the nebulae, and discuss their formation in the context of binary evolution.

2. Sample selection and morphological classification

2.1. Sample selection and visual inspection

We investigate the surroundings of stars belonging to four input samples in WISE 22 μm data (Wright et al. 2010). The main sample is taken from the BSC, a catalog of all stars with V magnitude 6.5 or brighter, and consists of all 3768 OBA stars (i.e., 1962 A stars, 1756 B stars, and 50 O stars). The BSC appears as a suitable source for this type of study. On the one hand, it contains enough stars to draw statistically significant conclusions, and on the other hand, the stars are bright enough to have been well studied in the literature. The sample is magnitude limited, not volume limited, meaning that the volume probed by O stars is much larger than that of B or A stars. More specifically, for a limiting V magnitude of 6.5, the heliocentric distance probed with an O5 star is 1500 pc, while the distance probed by an A5 star is smaller than 100 pc. The BSC sample serves as a comparison baseline for our population-restricted samples of Be stars, BeXRBs, and Be+sdO systems.

The Be sample consists of all known Be stars in the BSC as identified by Zorec & Briot (1997) or classified as such in SIMBAD (Wenger et al. 2007), resulting in 234 candidates. Additionally, we inspected a list of 72 BeXRBs (Raguzova & Popov 2005), and the Be+sdO sample of Wang et al. (2018) comprised of 5 known Be+sdO binary systems, 8 candidate, and 4 potential candidate systems. An overview of the different samples is given in Table 1.

In our analysis of the BSC sample, all selected stars were inspected twice. In the first iteration, we used the WISE 22 μm images as the nebulae tend to be most prominent there. Only the brightest nebulae at 22 μm are also visible at other wavelengths, especially at 12 μm (WISE W3) or H α . We checked for comple-

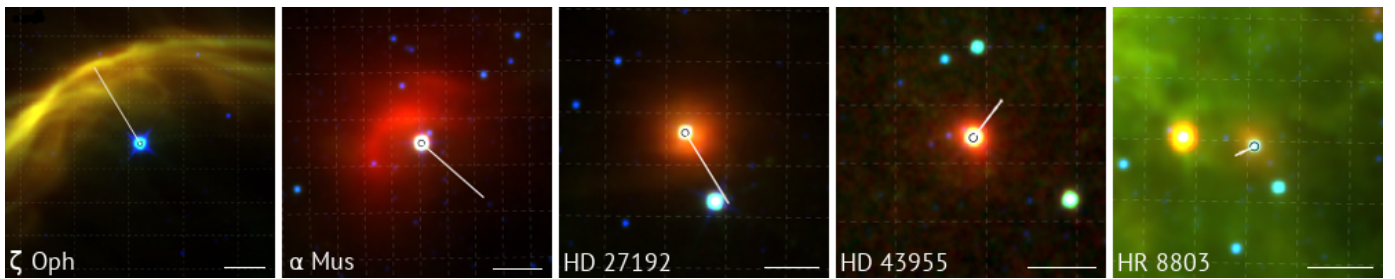


Fig. 1. Representative examples for each morphological group. From left to right: aligned bow shocks, unaligned bow shocks, and centered, unresolved, and not classified nebulae. All images are RGB images where red, green, and blue correspond to the WISE 22,12, and 4.6 μm filters. The straight white lines show the proper motion corrected to the local standard of rest. Their length indicates the displacement of each star within 10,000 yr. The white bar at the bottom of each panel corresponds to 2'.

Table 1. Overview of the inspected samples, where N_{stars} indicates the total number of stars in the sample (candidates are given in brackets). Fourteen of the Be+sdOs and four of the BeXRBs are also contained in the BSC sample, and all Be stars are part of it by definition.

Sample	N_{stars}	Source
Be stars	234	BSC / SIMBAD (Zorec & Briot 1997)
BeXRBs	72	Raguzova & Popov (2005)
Be+sdOs	5 (12)	Wang et al. (2018)
OBA stars	3768	BSC (Hoffleit & Jaschek 1991)

mentary H α images from the SuperCOSMOS H-alpha Survey (SHS Parker et al. 2005), but because of their rarity, we focused our investigation on the WISE data at 22 μm . The stars were examined by eye in image windows of 600" \times 600", while the flux cuts were changed manually depending on the particular field. In this step, 318 stars were identified that show a clearly extended emission in WISE W4.

In a second and independent iteration, all selected stars were examined again. The image windows were increased to 1200" \times 1200" to better evaluate the local surroundings. Here, we investigated not only the 22 μm images, but also RGB-images from the WISE data where the 22 μm band is shown in red, the 12 μm band in green, and the 3.4 μm band in blue.

During this second step, about 50 stars were rejected because the suspected extended IR emission could be identified as a second star very close to the target star becoming clear in the shorter wavelength bands. For the remaining 255 cases, we estimated fluxes and sizes of the nebulae from aperture photometry. As the nebulae exhibit different morphologies, the shape of each individual nebula was used instead of a circular aperture. This shape was determined by comparing the flux values in each pixel with the local background and its standard deviation σ . A pixel is defined to belong to the nebula when the flux was 10σ higher than the averaged background. These individual apertures were used to calculate the 22 μm flux of each nebula.

2.2. Morphological classification

We classified the extended emission with respect to the nebular morphology and the direction of proper motion of the stars. This is especially important for bow shocks (see Sect. 4.1.2). For these latter nebulae, we defined a misalignment angle α as the unsigned angle between the direction of proper motion of the star and the bow shock vector, connecting the position of the star with the apex of the bow shock.

We defined the following morphology groups (see Fig. 1), where the number in parentheses gives the final number of nebulae classified in this group:

- **Aligned bow shocks (34):** nebulae that have a sickle-like shape, a clear offset between the star and the nebula, and a misalignment angle $\alpha \leq 20^\circ$ (within the errors of the proper motion vector).
- **Unaligned bow shocks (60):** nebulae that have the sickle-like shape typical of bow shocks, a clear offset between the star and the nebula, but a misalignment angle $\alpha \geq 20^\circ$. This means that the apparent motion of the star is not aligned with the opening angle of the nebula.
- **Centered (52):** clearly extended and not sickle-shaped nebulae, where the star is situated within the extent of the nebula. The shapes are mostly roundish, elliptical, diffuse, or asymmetric, with a wide range of irregular morphologies.
- **Unresolved (72):** nebulae for which the image resolution in WISE is not good enough to classify the shape, that is, sickle-like shapes cannot be distinguished from round or circular nebulae. The lack of resolution means that no offset between nebula and star can be discerned.
- **Not classified (37):** nebulae that cannot be unambiguously classified into one of the other groups because of field crowding, background contamination, or both.

After defining the morphology groups, we checked for 24 μm data from the Multiband Imaging Photometer for Spitzer (MIPS, Rieke et al. 2004) for all 255 nebulae. MIPS has a point spread function (PSF) size of 6", thus twice the resolution as WISE (Rieke et al. 2004). Unfortunately, Spitzer did not perform an all-sky survey, so sky coverage is sparse and only 61 of the 255 nebulae found in WISE were observed by MIPS as well. In 25 of the 61 cases, the higher-resolution MIPS data allowed us to reclassify the nebular shape and estimate a misclassification error for the nebulae without MIPS data coverage.

Nineteen nebulae initially classified as aligned or unaligned bow shocks were observed with MIPS, but only in one case did the higher resolution lead to a reclassification. This indicates that the bow shock classification is robust at lower resolution as well, with a misclassification error of roughly 5%. For 23 nebulae classified as centered, higher resolution MIPS data were available, which in five cases revealed a previously hidden bow shock. This implies a misclassification rate for centered nebulae of 22%. Thirteen nebulae classified as unresolved in WISE have additional MIPS data. Six of the cases showed an offset in MIPS and revealed a bow shock not seen in the inspection of the WISE data, while three cases could be reclassified as centered nebulae, adding up to a reclassification in 70% of the cases. Five of the six not classified nebulae (i.e., 83%) observed by MIPS

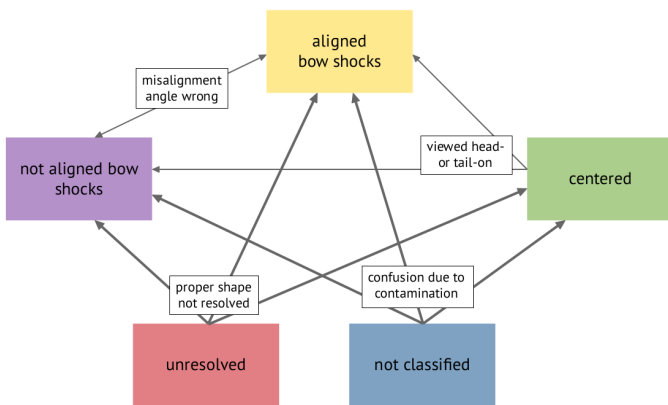


Fig. 2. Sketch of the possible misclassification paths between the defined morphology groups.

were reclassified into other groups. As expected, the classification of unresolved and not classified nebulae could be strongly improved by higher resolution data.

Figure 2 illustrates the possible misclassification paths arising from insufficient resolution. Additionally, bow shocks might have been classified as unaligned bow shocks and vice versa if the proper motion values taken from the literature were incorrect. This might be the case because for most of the stars, only Hipparcos (van Leeuwen 2007) proper motions are available. This error can be reduced with the 2nd Gaia data release, still pending at the time of writing, which should feature better proper motion values for the BSC stars.

For the statistical evaluation of the sample we set up a database containing literature information as well as the parameter values measured by us for all stars we found to be associated with nebulae. It is given in Tables B.1 and B.2 and can be accessed via the Centre de Données astronomiques de Strasbourg (CDS).

Table B.1 gives an overview over the parameters we gathered from the literature, including identifiers, coordinates, HD numbers, V-band magnitudes, and spectral types, taken from SIMBAD. Additionally, we provide parallaxes p , proper motions μ , and radial velocities v_{rad} with their respective errors for all available stars.

Table B.2 lists the parameters we derived. These include the final morphological classification we assigned to each nebula after inspection of the MIPS data and information about whether the star is a known Be star, has a nebulous spectrum, or is a known binary. We calculated distances d and measured angular sizes and total fluxes of the nebulae. For bow shocks and unaligned bow shocks, we give angular and linear distances $R(0)$ between the position of the star and the apex of the bow shock and misalignment angles α as defined above. Additionally, we calculated space velocities of the stars from literature values for distance d , proper motion μ , and radial velocity v_{rad} via

$$v_{\text{space}} = \sqrt{v_{\text{rad}}^2 + (4.744 \cdot \mu \cdot d)^2}. \quad (1)$$

Because of large errors both in distance and proper motion, we only give space velocities for stars for which the error in each individual measurement is $< 30\%$.

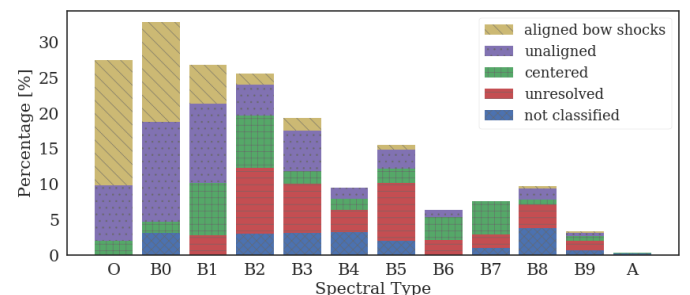


Fig. 3. Associations of different morphology groups with spectral types. Because of their low numbers, O and A stars are not divided into subtypes. The fractions are given with respect to the total number of stars of the respective spectral type in the BSC.

3. Results

3.1. BSC stars with nebulae

We find that 255 of all OBA stars in the BSC (i.e., $\sim 7\%$) have associated extended IR nebulae, visible in WISE data at $22\,\mu\text{m}$. Of these, 14 are associated with O stars, 234 with B stars, and 7 with A stars. Because of the strong dependency on spectral type of the stellar content of the BSC, the fraction of nebulae, however, declines strongly toward later spectral types: 28% of all O stars, but only 13% of the B and 0.4% of the A stars are associated with IR nebulae. Of the 7 A stars with nebulae, 3 are supergiants with luminosity classes Ia and Ib (HD 21389, HD 20041, and $\tau^2\,\text{Sco}$) while 1 ($\xi\,\text{Cep}$) is classified as spectroscopic binary in SIMBAD.

Absolute and relative abundances of the morphological types of IR nebulae defined in Sect. 2.2 are provided in Table 2. Fig. 1 shows a representative example of each morphological category. About 40% of all objects belong to the ambiguous groups of unresolved and not classified nebulae. The aligned bow shocks are the rarest objects in this sample, while 52 nebulae were classified as centered. Nebulae classified as centered might actually be bow shocks viewed head- or tail-on that appear roundish and centered on the star as a result of projection effects (see Sect. 4.1.5).

In Fig. 3 we show the association frequency of morphology types with spectral subtypes. The morphology types exhibit different dependencies on spectral type: The aligned bow shocks are the main reason for the overall decline in spectral type: while the fraction is highest for O stars, it decreases strongly toward later spectral types. Unaligned bow shocks are also less frequent around later-type stars, but the decline is not as strong as for the aligned bow shocks. Centered nebulae can be found at all spectral types with a peak around B1-B2.

As demonstrated in Fig. 4, we find an accumulation of nebulae along the Galactic plane as well as tracing Gould's Belt. Gould's Belt is a ring-like region tilted with respect to the Galactic plane by $16 - 20^\circ$, in which large OB associations are located, that is, the Orion, Ophiuchus, and Cygnus star-forming regions (Poppel 1997), which contain many young O and B stars and atomic and molecular gas (Perrot & Grenier 2003). However, the association with IR nebulae is not restricted to a narrow strip around the Galactic plane, and nebulae are also found at higher latitudes.

Figure 5 shows the space velocity distribution for each of the morphological categories. As mentioned in Sect. 2.2, we only calculated space velocities for the stars with individual errors in d , μ , and $v_{\text{rad}} < 30\%$. The total space velocity of stars associated with aligned bow shocks is on average higher than the veloc-

Table 2. Classification scheme based on the shape of the nebulae associated with BSC stars, the misalignment angle α , and the spatial offset between the star and the nebula. Columns 5 and 6 give the absolute number N_{neb} and the relative frequency f_{neb} of nebulae belonging to the respective groups. To estimate counting errors, we use the binomial error formula $\Delta f = \sqrt{(f(1-f)/N)}$ (not taking into account the misclassification errors). Here, we give the updated numbers and fractions after the reclassification based on the MIPS data. The last column indicates the potential formation mechanism (see Sect. 4.1).

Classification	Shape	α	offset	N_{neb}	f_{neb}	Potential formation mechanism
aligned bow shock	sickle-like	$\leq 20^\circ$	yes	34	$13 \pm 1\%$	high-velocity star
unaligned bow shock	sickle-like	$\geq 20^\circ$	yes	60	$24 \pm 1\%$	motion of ISM
centered	round/elliptical/diffuse	-	no	52	$20 \pm 1\%$	RLOF in binary system
unresolved	not resolved	-	no	72	$28 \pm 1\%$	-
not classified	ambiguous	-	-	37	$15 \pm 1\%$	-

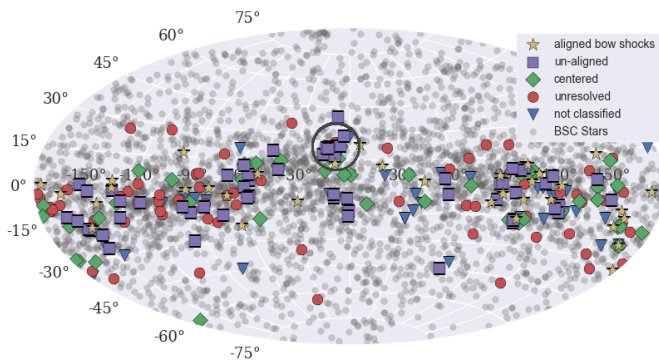


Fig. 4. Distribution of all O, B, and A stars in the BSC over the sky (gray dots, transparent for better visibility). The BSC stars associated with different morphological types of IR nebulae are identified with the symbols explained in the legend. The Ophiuchus star-forming region is marked by a circle.

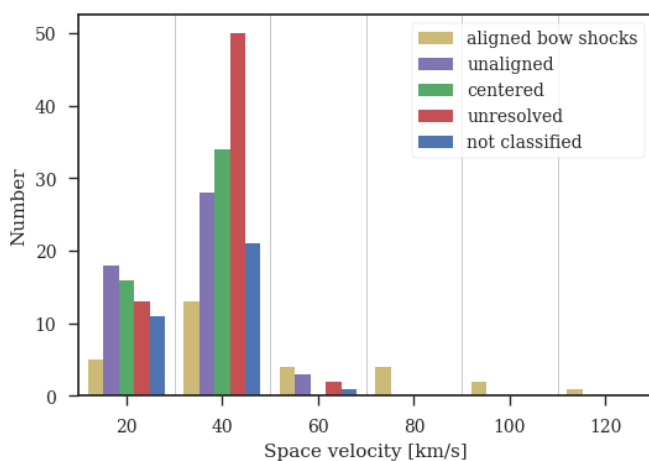


Fig. 5. Distribution of space velocities of the BSC stars calculated from Eq. 1. The colors correspond to the different morphological groups as indicated in the legend.

ity of the stars associated with other morphological types: all nebulae associated with stars with velocities higher than 60 km/s are aligned bow shocks. On the other hand, there are also a few aligned bow shocks around low-velocity stars. Centered nebulae can be found around stars with velocities of up to 40 km/s, while unresolved and not classified nebulae are associated with stars with velocities up to 60 km/s.

3.2. Subsamples

Here we investigate the stars included in the three subsamples defined in Sect. 2.1 for associations with IR nebulae. We employed the same inspection approach as for the BSC sample described in Sect. 2.1.

Be stars

Of the 234 inspected Be stars, 34 (i.e., 15%) are associated with IR nebulae. This can be compared to the fraction of normal B stars (excluding the Be stars) with associated nebulae, which is 13%. Among these 34 nebulae, there are 4 aligned bow shocks, 7 unaligned bow shocks, and 11 centered nebulae. This means that in total, 1% of all the Be stars are associated with aligned bow shocks, 3% with unaligned bow shocks, and 5% with centered nebulae.

More B stars in the BSC might be Be stars as the Be phenomenon is transient and might not be detected as such in observations with limited time coverage. This would influence the ratio between B and Be stars in the BSC and thus the comparison between the fraction of B and Be stars associated with nebulae. Eight Be stars with nebulae were also observed with MIPS. However, in none of these cases did the additional higher resolution data change the morphological classification.

BeXRBs

We investigated a total of 72 BeXRBs, among which we found 4 associations with IR nebulae and 15 uncertain cases. As BeXRBs are typically detected through their strong X-ray emission (see Sect. 1), they are observed to much larger distances than the typical B stars in the BSC sample. Only 4 BeXRBs are within the optical brightness limits of the BSC. Two of these are associated with an IR nebula: γ Cas (not classified) and μ^2 Cru (centered). The detection of the other 2 nebulae around BeXRBs, where the stars are too faint to be included in the BSC, should be considered with caution, as the stars are probably at much larger distances. Hence the risk of chance alignments with ISM structures increases, especially for objects relatively close to the Galactic plane. This is the case for γ Cas and μ^2 Cru: they are within $\pm 6^\circ$ of the Galactic plane. Only μ^2 Cru was observed by MIPS, but this did not change its morphological classification.

Be+sdOs

Of the 5 known Be+sdOs and the 12 candidate and potential candidate systems, 3 (HD 41335 and HD 214168, both centered, and ϕ Per, not classified) are associated with IR nebulae and 1 case is uncertain (59 Cyg, not classified). The clear detections

are also part of our BSC sample. Only for HD 41335 are MIPS data available that confirm the classification as centered nebulae.

The findings for these three subsamples are summarized in Table 3. Because of incompleteness of the input catalogs, the absolute numbers can only be lower limits, especially for the Be+sdO systems, which are difficult to identify. Absolute and relative numbers are of course subject to classificational uncertainties, as described in Sect. 2.2.

4. Discussion

4.1. BSC sample

4.1.1. Unresolved and not classified nebulae

As described in Sect. 2.2, about 70% of the nebulae unresolved by WISE may be resolved with a twice narrower PSF. Accordingly, about 47 or more of the total of 68 unresolved nebulae without MIPS data might be reclassified at higher resolution. Applying corresponding statistical corrections, we estimate that about 31 might be bow shocks, 16 might be centered nebulae, and 21 would still be unresolved. Their individual genuine character can, however, only be derived from higher-resolution data. The large number of unresolved nebulae with a space velocity $> 30 \text{ km/s}$ additionally indicates that a majority of them could be hidden bow shocks. In addition to the unresolved nebulae, we do not take into account the not classified nebulae in the following as in the context of this work no information can be drawn from them.

4.1.2. Aligned bow shocks

Bow shocks develop when the relative velocity between a star with a strong stellar wind and the local ISM is supersonic (see, e.g., van Buren & McCray 1988; Comerón & Kaper 1998; del Valle & Romero 2012). The size and brightness of a bow shock are defined mainly by three parameters: Theoretical modeling shows that a higher relative velocity as well as a higher density of the ambient ISM leads to smaller bow shocks, while their size increases with increasing wind strength and the thereby induced mass loss (Meyer et al. 2014, 2016). Stellar winds are generally stronger in more massive stars, leading to the expectation that bow shocks are more common and prominent around earlier-type stars. In the case of later-type (i.e., late-B and A-type) stars the radiation pressure on dust grains might lead to the formation of a bow shock (van Buren & McCray 1988; Ochsendorf et al. 2014).

Historically, the formation of a bow shock was attributed to a high stellar velocity with respect to its surroundings (van Buren et al. 1995; Kaper et al. 1997). The stars producing such bow shocks are called runaway stars and typically move at a high peculiar velocity $> 30 \text{ km s}^{-1}$ (Blaauw 1961; Gies & Bolton 1986). The runaway population is dominated by O stars (Stone 1991) that are observed outside of star-forming regions, indicating that they moved away from their place of formation (Silva & Napiwotzki 2011). Two possible mechanisms may lead to a high peculiar velocity: (i) expulsion from an SN-disrupted binary (see Sect. 1 and Blaauw 1961; Tauris & Takens 1998), and (ii) encounters between a close binary system and a tertiary star or another binary system in the parental cluster, which can lead to the ejection of one of the stars (Poveda et al. 1967). Observations indicate that both mechanisms are playing an important role (Hoogerwerf et al. 2000).

The alignment in our first morphological group between the motion of the stars and the sickle shape of the associated bow shocks implies that the associated stars are high-velocity stars. The steep decline with spectral type (see Fig. 3) agrees with the theoretical prediction that bow shocks are stronger around earlier-type stars as they have much stronger winds. A majority of the A stars with bow shocks are either supergiants or in a binary system. While MS A stars in general have no winds of any relevance, supergiants probably do have a wind strong enough for the formation of a bow shock (McCarthy et al. 1997). The recent observation of a bow shock around the red supergiant star IRC-10414 (Gvaramadze et al. 2014) further supports this.

Additionally, the decline with spectral type reflects the fact that the population of high-velocity stars is dominated by early-type stars. Most aligned bow shocks in our sample are associated with stars that have high space velocities (i.e., up to 120 km/s , see Fig. 5). A small number of outliers has $v_{\text{space}} < 30 \text{ km/s}$, probably indicating that in these cases the ISM motion dominates the relative motion and is by chance aligned with the stellar motion (see next subsection).

Because the velocity gain of at least some runaway stars arises from their binary origin, the 34 stars with bow shock nebulae (i.e., 13% of all the stars with nebulae) can be placed in the context of binary evolution. Additionally, by using aligned bow shocks as indicators of high-velocity stars, we can crudely estimate their fraction in our limited sample of 50 O stars. We find 9 associations between O stars and aligned bow shocks, that is, almost 20%. This agrees well with other studies that found a high-velocity star fraction between 10% (Blaauw 1961; Gies & Bolton 1986) and 27% (Tetzlaff et al. 2010).

4.1.3. Unaligned bow shocks

Recent observational studies showed that bow shocks are not restricted to stars that move with high space velocities (Povich et al. 2008; Kobulnicky et al. 2016). Large-scale motions within the ISM can also be responsible for high relative velocities between star and ISM (Povich et al. 2008). Our morphological group of unaligned bow shocks supports this finding: stellar motion with respect to the ISM cannot be the driving force in the formation of these bow shocks.

As described in Sect. 3.1, unaligned bow shocks are associated with all spectral types we studied. This agrees well with theory: The main part in this interaction is the motion of the ISM, not stellar motion. As described before, O stars are favored as nuclei of bow shocks for two reasons: their strong winds, and high velocities. While the role of the wind should not depend much on the stellar space velocity with respect to the ambient ISM, the velocity threshold for the occurrence of bow shocks is obviously lower if the ISM also contributes much to the relative velocity between star and ISM. It is therefore not surprising that the fraction of early-type B stars with unaligned IR nebulae, which have weaker winds, is larger than that of aligned bow shocks (Fig. 3). In B stars in general, the formation of a bow shock depends more strongly on the ISM contribution to the relative velocity. This is confirmed by the distribution of space velocities of the stars with unaligned bow shocks: as shown in Fig. 5, the space velocity of these stars is in general significantly lower than for the aligned bow shocks, that is, mostly $< 40 \text{ km/s}$.

Unaligned bow shocks can be used as tracers of large-scale ISM motions (Kiminki et al. 2017). Such motions are common in star-forming regions where they are created by the copious winds of hot stars (Kudritzki & Puls 2000) and multiple previous SN explosions (de Avillez & Breitschwerdt 2010). The Ophi-

Table 3. Number of nebulae classified in the morphology groups defined in Sect. 2.2 and associated with stars in the subsamples. The first column refers to the classification in shape. The subsequent columns give absolute number and relative frequency of nebulae belonging to the Be star, BeXRB, and Be+sdO samples, respectively. Counting errors are estimated with the binomial error formula $\Delta f = \sqrt{(f(1-f)N}$. The last column indicates the potential formation mechanism (see Sect. 4.1).

Classification	Be stars		BeXRBs		Be+sdOs		Potential formation mechanism
	N_{neb}	f_{neb}	N_{neb}	f_{neb}	N_{neb}	f_{neb}	
aligned bow shocks	4	$12 \pm 2\%$	-	-	-	-	high-velocity star
unaligned bow shock	7	$21 \pm 3\%$	-	-	-	-	motion of ISM
centered	11	$32 \pm 3\%$	1	$25 \pm 5\%$	2	$67 \pm 11\%$	RLOF in binary system
unresolved	6	$18 \pm 2\%$	-	-	-	-	-
not classified	6	$18 \pm 2\%$	3	$75 \pm 5\%$	1	$33 \pm 11\%$	-

uchus star-forming region, for example, clearly shows an overabundance of unaligned bow shocks (encircled in Fig. 4). Accordingly, the defining link between bow shocks and high stellar velocity is relaxed. The basic physics of aligned and unaligned bow shocks, however, remains the same because of the roughly spherical symmetry of the stellar winds.

4.1.4. Comparison to Kobulnicky et al. 2016

Kobulnicky et al. (2016) carried out a comprehensive visual inspection of existing space-based imaging IR surveys, and presented a new catalog of candidate bow shock nebulae containing 708 objects. In a follow-up paper, they performed aperture photometry and derived spectral energy distributions (SEDs) for all the objects (Kobulnicky et al. 2017). For candidate bow shocks, the authors imposed the following classification criteria: the nebulae must have an arc shape, a high degree of symmetry, and at least one prominent star located near the axis of symmetry. Subsequently, they classified the detected nebulae into four groups depending on their environment: bow shocks located in apparently isolated environments (70% of all nebulae), facing H II regions, facing bright-rimmed clouds, and located within H II regions. They called the latter "in situ" bow shocks, indicating that these bow shocks do not originate from the fast motion of a high-velocity star, but from ISM motion.

Reliable proper motion data are only available for $\sim 20\%$ of their stars. In one-quarter of the latter, the position angle of the bow shock is found to be aligned with the direction of the proper motion. This value is lower than the fraction of aligned bow shocks (34) of all bow shocks (94) in the BSC, which is 36%. It has to be noted, however, that Kobulnicky et al. defined bow shocks as aligned if the misalignment angle α is $\leq 45^\circ$, while our cutoff is $\leq 20^\circ$. Their derived fraction of aligned bow shocks is nevertheless lower than ours, which might at least partly be explained by the fact that, in contrast to our study, their proper motion vectors were not corrected for the local standard of rest.

The approaches used by Kobulnicky et al. and by us are complementary to each other: Kobulnicky et al. searched for IR nebulae with bow shock morphologies, classified them according to their environment, and then studied their association with stars, whereas we searched all OBA stars in the BSC for an associated IR nebula. Therefore, our analysis permits inferences to be made not only about the incidence of strong interactions between stellar winds and the ISM, but also about ISM-independent processes that may lead to the formation of IR nebulae associated with OBA stars. Moreover, Kobulnicky et al. inspected archival MIPS images mostly covering the inner Galactic plane at latitudes between $|b| \leq 1^\circ$, and complementary WISE data at latitudes up to $|b| \leq 2^\circ$. In contrast, our study covers the whole sky (therefore it mostly depends on the lower resolution WISE data),

but is not restricted to bow shocks. We start from a (magnitude-limited) sample of bright stars of spectral types O, B and A and search for associated nebulae of any morphology.

A comparison between the nebulae found by Kobulnicky et al. and our sample yields only a small overlap of 11 stars (5 aligned and 6 unaligned bow shocks; by definition of the Kobulnicky et al. sample, there are no common objects with other structures). Of these 11, 10 fall into Kobulnicky et al.'s category of "isolated" environments (as the majority of their sample, i.e., 70%), and 1 unaligned bow shock is "facing an H II region". As mentioned in Sect. 3.1, we only have 14 O stars associated with IR nebulae in our sample. It is thus interesting to note that 5 of the 11 stars in the overlap are associated with O type stars and the rest are associated to B0 stars. A possible reason for the restriction of common objects to very early-type stars could be the clustering of these objects around the Galactic plane. The overall small overlap could be due to the different input data: while our search includes all OBA stars within a certain brightness limit in the whole sky, Kobulnicky et al. focused on a small region close to the Galactic plane without taking into account the spectral type or brightness of the associated star.

4.1.5. Centered nebulae

Our third morphology group consists of all nebulae in which the emission is centered on the star. The shape of these nebulae is circular, elliptical, or diffuse. Possible explanations for the formation of IR nebulae without obvious offset from the associated star include the following.

- Some of the centered nebulae could be bow shocks viewed head- or tail-on. Their associated stars should exhibit small proper motions, that is, low tangential velocities, but fast radial velocities. We calculated space velocities for 50 of the 52 centered nebulae (the remaining 2 were omitted because of high uncertainties in distance and proper motion, see Sect. 2.2). Of these 50, only 2 stars have a high tangential velocity $v_{\tan} > 30$ km/s, while 2 others have radial velocities $v_{\text{rad}} > 30$ km/s. Additionally, the abundance of associations with centered nebulae depends on spectral type. A peak is visible at spectral types B1/B2, implying that not all centered nebulae are bow shocks viewed head- or tail-on.

In Appendix A we compare the distribution of apex distances of bow shocks to the distribution of radii of centered nebulae. We calculated the radii from the physical sizes of the nebulae assuming that all nebulae have a circular shape. As the centered nebulae are not all spherically symmetric, and because the measured apex distance is a projected quantity, we do not expect the underlying distributions to be similar. We tested the similarity of the two distributions by means

of a Kuiper test, which indicated that we cannot distinguish between them at a 2σ level.

Acreman et al. (2016) computed synthetic IR emission maps for bow shocks viewed at inclination angles 30° , 60° , and 90° smoothed to the resolution of WISE W4 (see their Fig. 3). The authors found a "noticeable asymmetry" of the nebula "with a peak ahead of the star" already at an inclination of 30° **that becomes** a more clearly identifiable bow shock at higher inclinations. We thus assume that bow shocks seen under inclination angles $\leq 30^\circ$ appear spherical with WISE. Assuming a continuous distribution of bow shock orientations in the sky, the fraction of bow shocks viewed head- or tail-on is given by the integral of a random distribution of angles from 0° to 30° , that is, $1 - \cos(30^\circ) = 13\%$. This implies that at least 13% of all bow shock nebulae would be classified as centered nebulae because of their head- or tail-on orientation. This indicates that the 94 bow shock nebulae we found correspond to 87% of the total bow shock population (i.e., 108 nebulae), and that at least 11 centered nebulae should be bow shocks viewed head- or tail-on. Applying this additional possible misclassification to all centered nebulae statistically reduces their number from 52 to at most 41, that is, 16% of all nebulae.

- The IR emission could arise in the remains of the parental disk in which the star formed. However, these disks are transient structures with lifetimes on the order of a few million years. The lifetimes steeply decrease with the mass of the star (see, e.g., De Marchi et al. 2013; Pfalzner et al. 2014) because the strong stellar irradiation leads to disk dissipation (Haisch et al. 2001). This is much shorter than the typical MS lifetime of early-type stars (e.g., $\sim 2 \cdot 10^8$ yr for B5V, Ekström et al. 2012). Moreover, protostellar disks are smaller than $1000 \text{ AU} \approx 5 \cdot 10^{-3} \text{ pc}$ (Williams & Cieza 2011), whereas the typical radii of the observed IR nebulae of 0.5 pc are 100 times larger.

- The nebulae could be the remnants of a supernova explosion of a companion star. For a typical radius of 0.5 pc of the IR nebulae in question and typical expansion velocities of supernova remnants (5,000 km/s, Hayato et al. 2010), putative SN explosions would have taken place 100 years ago, i.e. during historical times. A typical absolute luminosity of core-collapse SNe is -17 mag in V (Richardson et al. 2014), which is about 14 mag brighter than that of a B1 V star (Wegener 2006). Therefore, even the faintest B1V star in the BSC at $m_V = 6.5$ would have shone at $M_V = -7.5$ around maximum, which is 10,000 times brighter than Sirius. There is no record of such events.

- The IR emission could arise in surrounding dust that is heated by the star. This could either be dense ISM clouds that are independent of the star, or dust formed by the star itself. Additional observations of one peculiar nebula around a classical Be star, HD 303056 (classified as B3 in SIMBAD), indicated a nebular density of $n_{\text{neb}} = 56 \pm 5 \text{ cm}^{-3}$ (Bodensteiner, Master thesis, unpublished; Bodensteiner et al., in prep.). The typical density of the ISM, however, is $n_{\text{ISM}} \approx 1 \text{ cm}^{-3}$ (Ferriere 2001). Therefore, if this dust is unrelated to the star and part of the ISM, the density of the latter would have to be accidentally increased by nearly two orders of magnitude, which seems very unlikely.

Figure 4 demonstrates that the association of nebulae is not restricted to a narrow strip around the Galactic plane. It extends to higher Galactic latitudes, showing that such nebulae do not only occur in regions of dense ISM where the probability of both physical and apparent associations is highest.

This suggests that some of the IR nebulae without bow-shock appearance may not require the ISM, but are formed by the associated stars in some other way.

Two basic conditions must be fulfilled in stars in order to produce dust: the temperature of the material must be below the dust condensation temperature of around 1500 K (Hoefner et al. 1998), and the density must be high (Andersen 2007). These conditions are fulfilled for example in AGB stars (Ferrarotti & Gail 2006), or in evolved massive stars like luminous blue variables (LBVs) or Wolf-Rayet (WR) stars (Toalá et al. 2015).

The mass-loss rate of AGB stars is between 10^{-8} and $10^{-4} M_\odot \text{ yr}^{-1}$ (Habing 1996; Kemper et al. 2001), leading to the formation of circumstellar nebulae (Wood et al. 2004; Suh 2004). LBVs show stellar outbursts and episodes of high mass loss during which the stars lose significant fractions of their initial mass (Humphreys & Davidson 1994; Smith 2014). The wind mass loss rates of LBVs is typically 10^{-5} to $10^{-4} M_\odot \text{ yr}^{-1}$ (Lamers & Fitzpatrick 1988; Smith et al. 2004; Groh et al. 2009). Several dusty nebulae are known around LBVs (Weis 2003; Gvaramadze et al. 2009).

The mass loss in MS B stars is in general very small compared to these numbers. B0 stars can have a mass loss of up to $10^{-9} M_\odot \text{ yr}^{-1}$. This number, however, decreases strongly with effective stellar temperature. Below 15 000 K, no homogeneous line-driven wind is possible (Krticka 2014), making the mass loss completely ineffective in terms of the formation of such nebulae.

- The IR nebulae could be formed by non-conservative mass transfer during RLOF or in a stellar merger. Depending on the type of interaction, the remaining star would be effectively single (i.e., when the two components have merged) or have a compact companion (i.e., a WD, sdO, NS, or even a BH). As the least massive of these compact companions, WDs and sdOs, are hard to detect, many of them, if they exist, may have remained undetected. The nebulae would then become visible because the ejected material is heated by the absorption of photons from the OB star, and in the case of RLOF, additionally by the compact companion. These compact companions, especially sdOs, have very high temperatures and thus emit around 100 times more highly energetic photons than an early-type star (the number of ionizing photons for an sdO is 10^{48} s^{-1} (Gotberg et al. 2017), while a B1 type star with an effective temperature of $\sim 26\,000$ K typically emits 10^{46} s^{-1} (Diaz Miller et al. 1998). Additionally, the temperature of sdOs remains high for a long time, increasing the visibility period of such nebulae.

This, perhaps still incomplete, multitude of possibilities shows that centered nebulae do not have a unique straightforward explanation. We can exclude that they are the remains of the parental disk or remnants of a previous SN explosion of a possible companion star, however. Because of the negligible mass loss of the stars in comparison to known dust-producing stars like AGBs, LBVs, or WR stars, it also seems unlikely that single stars produced the dust. Finally, some of the centered nebulae could be bow shocks viewed head- or tail-on.

In conclusion, we propose that the formation of most of the remaining centered nebulae (i.e., 16% of all nebulae) is related to binary interactions by non-conservative mass transfer either during RLOF or a stellar merger.

4.2. Subsamples

4.2.1. Be stars

The search for nebulae within the Be subsample yields three main results. First, we find a similar fraction of nebulae around Be stars as around normal B stars. This indicates that the presence of a circumstellar disk, which is the main characteristics of a Be star, is not significantly causal for the presence of an IR nebula.

Second, the fraction of centered nebulae around Be stars is marginally higher than around normal B stars. While 11 of the 34 Be stars, that is, 32%, are found to be associated with centered nebulae, this holds only for 39 of the 200 normal B stars (excluding Be stars) in the BSC, that is, 20%. The B stars in the BSC also include supergiants with strong winds. Therefore, if the distribution of space velocities of B and Be stars is about the same, the smaller percentage of Be stars with centered nebulae confirms that winds are not generally important for the formation of centered nebulae.

Third, four Be stars are associated with aligned bow shocks. Berger & Gies (2001) found the fraction of high-velocity stars among Be stars to be slightly higher than the fraction among normal early-type B stars (i.e., 3%-7% in comparison to $\approx 2\%$). They concluded that the existence of high-velocity Be stars indicates that at least some of the Be stars are formed in binaries. This is in agreement with our conclusion: the four Be stars with bow shocks probably gained their high velocity in previous binary interactions.

In total, this indicates that 11 + 4 out of 234 inspected Be stars, that is, 6%, are associated with nebulae that can be linked to binary interactions. In comparison, we found 39 centered nebulae + 20 aligned bow shocks associated with the 1522 normal B-type stars in the BSC, implying a fraction of 4%. The absolute numbers of star-nebula pairs and the corresponding fractional difference between Be and B stars, 6% vs. 4%, are small, however. Therefore, on the basis of our data, we cannot claim to see strong evidence that binarity is the physical cause of the Be star phenomenon.

The first detection of an elongated, asymmetric IR nebula in WISE data at $22\mu\text{m}$ around a Be star was 48 Lib (B3 IVe; Griffith et al. 2015), a shell star (i.e., viewed equator-on; Hanuschik & Vrancken 1996). Interferometric observations constrained the orientation in space (i.e., the tilt angle with respect to the plane of the sky) of this circumstellar decretion disk (Pott et al. 2010), while its position angle was determined by linear polarimetry (Štefl et al. 2012). Despite a difference in size of 5 orders of magnitude, the IR nebula visible in WISE seems to be parallel (Griffith et al. 2015) to the circumstellar decretion disk, indicating a common axis of rotation.

Recently, an elliptical, that is, centered nebula around the classical Be star HD 303056 was discovered in MIPS data at $24\mu\text{m}$ by Vasilii Gvaramadze (priv. comm.), which we will investigate in detail in a follow-up paper (Bodensteiner et al., in prep.). The presence and characteristics of such circumstellar nebulae around Be stars could give further indications pointing toward their binary origin.

4.2.2. BeXRBs and Be+sdO systems

No aligned bow shocks were found around BeXRBs and Be+sdO systems. As discussed above, aligned bow shocks are formed by high-velocity stars, whereas the standard process of formation of BeXRBs and Be+sdO systems, mass transfer dur-

ing RLOF, does not impart great velocity kicks to the systems. BeXRBs and Be+sdO systems are thus still bound in the original binary system. In the case of BeXRBs, this indicates that the binary system was not disrupted in the SN explosion of the companion.

The centered nebulae associated with one BeXRB and two Be+sdO systems might be the left-over material lost in previous binary interactions in which the primary star evolved into a compact object and the secondary was spun up to become a Be star. The low numbers, however, prevent us from any further statistical inferences.

5. Conclusions

We discovered a large number of IR nebulae associated with early-type stars. In addition to 4 BeXRBs, 3 Be+sdO systems, and 34 Be stars (with mostly unknown binary status) with extended IR nebulae, we detected 255 nebulae around OBA stars in the Bright Star Catalogue.

Among the 255 nebulae around BSC stars, we find that 94 nebulae have the typical sickle-like shape of a bow shock that forms when the relative velocity between star and surrounding ISM is supersonic. They can be subdivided into two groups: the first group, accounting for 13% of all nebulae, are bow shocks formed by high-velocity stars that probably gained their high velocity through close binary interactions. The second group (24%) supports the recent development in the understanding of bow shock formation. The missing alignment between proper motion and position angle of the apex of the bow shock indicates that not only a high stellar velocity, but also large-scale motions of the ISM produce bow shocks. This leads us to the assumption that in stars with aligned bow shocks, we see the combined effect of strong wind and high space velocity, while in not-aligned bow shocks, the high space velocity of the star itself is less relevant than the turbulent ISM motion. This is in agreement with the findings by Kobulnicky et al. (2016) and demonstrates that unaligned bow shocks can be used as tracers for large-scale ISM motions.

Using aligned bow shocks as indicators for high-velocity stars, we find a high-velocity star fraction of almost 20% in our limited sample of O stars. This agrees with earlier findings of Blaauw (1961), Gies & Bolton (1986), and Tetzlaff et al. (2010), for instance.

Furthermore, 52 centered nebulae have round, elliptical, or diffuse shapes. While $\sim 13\%$ might be bow shocks viewed head- or tail-on, this explanation does not hold for the majority. We can exclude that the IR emission arises in the remains of the parental disk, and also that the nebulae are remnants of the SN explosion of a former companion star. Because of their low mass-loss rates, single MS B and A stars do not form dust. MS O stars and B and A supergiants can have a higher mass loss. They account only for a small fraction of the whole sample, however.

Finally, we propose that the remaining centered nebulae, that is, 16% of all nebulae, are formed in the context of previous binary interactions. The observed IR nebulae might be explained through dust formed during non-conservative mass transfer (either RLOF or a stellar merger) that is heated by the OBA star (and a compact companion, if merging was avoided). Such nebulae should show elevated metal abundances due to their formation history and have a short lifetime because of their expansion.

In total, we can conclude that (16+13)%, that is, about one-quarter to one-third, of the nebulae detected around OBA stars in the BSC can be placed in the context of binary evolution. On the one hand, they can be seen as an indication of the velocity gain

by binary interaction leading to the formation of a bow shock. On the other hand, the nebulae can be direct observational evidence of the material lost in non-conservative mass transfer (i.e., in RLOF or a stellar merger) heated by the star (and a compact companion). Applying this to the number of O, A, and B stars in the BSC, we find that 8% of all O stars in the BSC, 4% of all B stars in the BSC, and 0.1% of all the A stars in the BSC are associated with IR nebulae that can be placed in the context of binary evolution. A majority of the A stars is, however, not single or not on the MS. The small difference between the fraction of B (4%) and Be stars (6%) with probably binarity-related companion IR nebulae is not significant enough to postulate a dominance of binarity in the formation of Be stars.

Our results encourage us to use the associations of IR nebulae with massive MS stars as a general tracer of past binary interactions. This could be further exploited by spectroscopic searches for companion stars. Companion detections would not only corroborate the conclusions of this paper, but would have the potential to give important new insights into the physical processes taking place in the different so far still poorly understood binary evolution and interaction channels.

Acknowledgements. We are particularly grateful to Vasilii Gvaramadze in pointing out the mid-IR nebula around HD 303056, which initiated this study, and to Thomas Rivinius and Alex C. Carciofi for helpful discussions during early stages of the project. We would like to thank Hugues Sana and Cole C. Johnston for valuable discussions concerning the paper and the referee for very helpful comments and suggestions. J.B. acknowledges support from the FWO_Odysseus program under project G0F8H6N. This publication makes use of data products from the Wide-field Infrared Survey Explorer, which is a joint project of the University of California, Los Angeles, and the Jet Propulsion Laboratory/California Institute of Technology, funded by the National Aeronautics and Space Administration. This work is partly based on archival data obtained with the Spitzer Space Telescope, which is operated by the Jet Propulsion Laboratory, California Institute of Technology under a contract with NASA. Support for this work was provided by an award issued by JPL/Caltech. This research has made use of the SIMBAD database, operated at CDS, Strasbourg, France and of NASA's Astrophysics Data System Bibliographic Services.

References

- Acreman, D. M., Stevens, I. R., & Harries, T. J. 2016, MNRAS, 456, 136
 Andersen, A. C. 2007, in Why Galaxies Care About AGB Stars: Their Importance as Actors and Probes, ed. F. Kerschbaum, C. Charbonnel, & R. F. Wing (Astronomical Society of the Pacific), 170
 Baade, D., Pигулский, А., Ривиниус, Т., et al. 2017, eprint arXiv:1708.07360
 Berger, D. H. & Gies, D. R. 2001, ApJ, 555, 364
 Blaauw, A. 1961, Bull. Astron. Inst. Netherlands, 15, 265
 Bodenheimer, P. 1995, ARA&A, 33, 199
 Carciofi, A. C., Okazaki, A. T., le Bouquin, J.-B., et al. 2009, A&A, 504, 915
 Casares, J., Negueruela, I., Ribó, M., et al. 2014, Nature, 505, 378
 Collins, G. W. 1987, in Physics of Be stars, ed. A. Slettebak & T. Snow, 3–19
 Comerón, F. & Kaper, L. 1998, A&A, 338, 273
 Comerón, F. & Pasquali, A. 2007, A&A, 467, L23
 de Avillez, M. A. & Breitschwerdt, D. 2010, in PASP Conf. Ser., ed. R. Kothes, T. L. Landecker, & A. G. Willis, 313
 De Marchi, G., Panagia, N., Guarcello, M. G., & Bonito, R. 2013, MNRAS, 435, 3058
 de Mink, S. E., Cantiello, M., Langer, N., et al. 2009, A&A, 497, 243
 de Mink, S. E., Langer, N., Izzard, R. G., Sana, H., & de Koter, A. 2013, ApJ, 764, 17
 de Mink, S. E., Sana, H., Langer, N., Izzard, R. G., & Schneider, F. R. N. 2014, ApJ, 782, 8
 del Valle, M. V. & Romero, G. E. 2012, A&A, 543, 10
 Diaz Miller, R. I., Franco, J., & Shore, S. N. 1998, ApJ, 501, 192
 Ekström, S., Georgy, C., Eggenberger, P., et al. 2012, A&A, 537, 18
 Ekström, S., Meynet, G., Maeder, A., & Barblan, F. 2008, A&A, 478, 467
 Ferrarotti, A. S. & Gail, H.-P. 2006, A&A, 447, 553
 Ferriere, K. M. 2001, Reviews of Modern Physics, 73, 1031
 Gies, D. R. & Bolton, C. T. 1986, ApJS, 61, 419
 Glebbeek, E., Gaburov, E., Portegies Zwart, S., & Pols, O. R. 2013, MNRAS, 434, 3497
 Gontcharov, G. A. 2006, Astronomy Letters, 32, 759
 Gotberg, Y., de Mink, S. E., & Groh, J. H. 2017, A&A, 608, 22
 Griffith, R. L., Wright, J. T., Maldonado, J., et al. 2015, ApJS, 217, 34
 Groh, J. H., Hillier, D. J., Damineli, A., et al. 2009, ApJ, 698, 1698
 Gvaramadze, V. V., Kniazev, A. Y., & Fabrika, S. 2009, MNRAS, 405, 1047
 Gvaramadze, V. V., Menten, K. M., Kniazev, A. Y., et al. 2014, MNRAS, 437, 843
 Haberl, F. & Sasaki, M. 2000, A&A, 359, 573
 Habing, H. 1996, A&ARv, 7, 97
 Haisch, K. E., Lada, E. A., & Lada, C. J. 2001, AJ, 121, 2065
 Han, Z., Podsiadlowski, P., Maxted, P. L. F., Marsh, T. R., & Ivanova, N. 2002, MNRAS, 336, 449
 Hanuschik, R. W. & Vrancken, M. 1996, A&A, 312, L17
 Hayato, A., Yamaguchi, H., Tamagawa, T., et al. 2010, ApJ, 725, 894
 Heber, U. 2009, ARA&A, 47, 211
 Heber, U. 2016, PASP, 128, 082001
 Hoefner, S., Jorgensen, U. G., Loidl, R., & Aringer, B. 1998, A&A, 340, 497
 Hoffleit, D. & Jaschek, C. 1991, The Bright star catalogue, 5th edn., ed. D. Hoffleit & C. Jaschek
 Hoogerwerf, R., de Bruijne, J. H. J., & de Zeeuw, P. T. 2000, ApJ, 544, L133
 Huang, W., Gies, D. R., & McSwain, M. V. 2010, ApJ, 722, 605
 Humphreys, R. M. & Davidson, K. 1994, PASP, 106, 1025
 Iben, Icko, J. & Livio, M. 1993, PASP, 105, 1373
 Ivanova, N., Justham, S., Chen, X., et al. 2013, ARA&A, 21, 59
 Kahabka, P. & van den Heuvel, E. P. J. 1997, ARA&A, 35, 69
 Kaper, L., van Loon, J., Augusteijn, T., et al. 1997, ApJ, 475, L37
 Kemper, F., Waters, L. B. F. M., de Koter, A., & Tielens, A. G. G. M. 2001, A&A, 369, 132
 Kenyon, S. J. & Webbink, R. F. 1984, ApJ, 279, 252
 Kharchenko, N. V., Scholz, R. D., Piskunov, A. E., Röser, S., & Schilbach, E. 2007, Astronomische Nachrichten, 328, 889
 Kiminki, M. M., Smith, N., Reiter, M., & Bally, J. 2017, MNRAS, 468, 2469
 Kippenhahn, R. & Weigert, A. 1967, Zeitschrift für Astrophysik, 65, 251
 Kobulnicky, H. A., Chick, W. T., Schurhammer, D. P., et al. 2016, ApJS, 227, 18
 Kobulnicky, H. A., Schurhammer, D. P., Baldwin, D. J., et al. 2017, AJ, 154, 18
 Krticka, J. 2014, A&A, 564, 10
 Kudritzki, R.-P. & Puls, J. 2000, ARA&A, 38, 613
 Lamers, H. J. G. L. M. & Fitzpatrick, E. L. 1988, ApJ, 324, 279
 Langer, N. 2012, ARA&A, 50, 107
 Lee, U., Saio, H., & Osaki, Y. 1991, MNRAS, 250, 432
 Martayan, C., Frémat, Y., Hubert, A.-M., et al. 2007, A&A, 462, 683
 Martin, R. G., Tout, C. A., & Pringle, J. E. 2009, MNRAS, 397, 1563
 McCarthy, J. K., Kudritzki, R., Lennon, D. J., Venn, K. A., & Puls, J. 1997, ApJ, 482, 757
 McSwain, M. V. & Gies, D. R. 2005, ApJS, 161, 118
 Meyer, D. M. A., Mackey, J., Langer, N., et al. 2014, MNRAS, 444, 2754
 Meyer, D. M. A., van Marle, A. J., Kuiper, R., & Kley, W. 2016, MNRAS, 459, 1146
 Ochsendorf, B. B., Cox, N. L. J., Krijt, S., et al. 2014, A&A, 563, 16
 Packet, W. 1981, A&A, 102, 17
 Paczynski, B. 1976, in Structure and Evolution of Close Binary Systems, ed. P. Eggleton, S. Mitton, & J. Whelan (Cambridge University Press), 75
 Parker, Q. A., Phillipps, S., Pierce, M. J., et al. 2005, MNRAS, 362, 689
 Perrot, C. A. & Grenier, I. A. 2003, A&A, 404, 519
 Petrovic, J., Langer, N., & van der Hucht, K. A. 2005, A&A, 435, 1013
 Pfalzner, S., Steinhausen, M., & Menten, K. 2014, ApJL, 793, 5
 Podsiadlowski, P., Joss, P. C., & Hsu, J. J. L. 1992, ApJ, 391, 246
 Pols, O., Cote, J., Waters, L. B. F. M., & Heise, J. 1991, A&A, 241, 419
 Poppel, W. 1997, Fundamentals of Cosmic Physics, 18, 1
 Portegies Zwart, S. F. 1995, A&A, 296, 691
 Pott, J. U., Woillez, J., Ragland, S., et al. 2010, ApJ, 721, 802
 Pourbaix, D., Tokovinin, A. A., Batten, A. H., et al. 2004, A&A, 424, 727
 Poveda, A., Ruiz, J., & Allen, C. 1967, Boletín de los Observatorios de Tonantzintla y Tacubaya, 4, 86
 Povich, M. S., Benjamin, R. A., Whitney, B. A., et al. 2008, ApJ, 689, 242
 Raghuzova, N. V. & Popov, S. B. 2005, Astronomical and Astrophysical Transactions, 24, 151
 Rappaport, S. & van den Heuvel, E. P. J. 1982, in Be stars; Proceedings of the IAU Symposium, ed. M. Jaschek & H. G. Groth, Vol. 98 (Cambridge University Press), 327–344
 Reig, P. 2011, Astrophysics and Space Science, 332, 1
 Richardson, D., Jenkins, R. L., Wright, J., & Maddox, L. 2014, ApJ, 147, 11
 Rieke, G. H., Young, E. T., Engelbracht, C. W., et al. 2004, ApJS, 154, 25
 Rivinius, T., Baade, D., Steffl, S., et al. 1998, in ASP Conference Series, ed. P. Bradley & J. Guzik, Vol. 135 (Astronomical Society of the Pacific), 343
 Rivinius, T., Carciofi, A. C., & Martayan, C. 2013, A&ARv, 21, 69
 Robinson, E. L. 1976, ARA&A, 14, 119
 Sana, H., de Mink, S. E., de Koter, A., et al. 2012, Science, 337
 Schneider, F. R. N., Podsiadlowski, P., Langer, N., Castro, N., & Fossati, L. 2016, MNRAS, 457, 2355

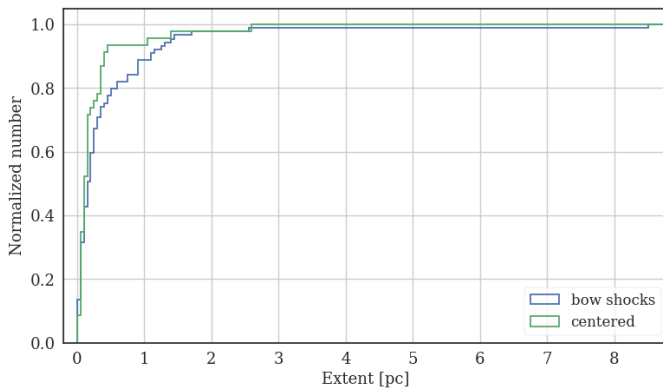


Fig. A.1. Normalized cumulative distribution of apex distances of bow shocks (blue) and radii of centered nebulae (green, assuming that all of them are spherical symmetric).

- Schootemeijer, A., Gotberg, Y., de Mink, S. E., Gies, D. R., & Zapartas, E. 2018, eprint arXiv:1803.02379
 Shao, Y. & Li, X.-D. 2014, ApJ, 796, 13
 Shu, F. H. & Lubow, S. H. 1981, ARA&A, 19, 277
 Sills, A., Adams, T., & Davies, M. B. 2005, MNRAS, 358, 716
 Silva, M. D. V. & Napiwotzki, R. 2011, MNRAS, 411, 2596
 Smith, N. 2014, ARA&A, 52, 487
 Smith, N., Vink, J. S., & de Koter, A. 2004, ApJ, 615, 475
 Štefl, S., Bouquin, J. B. L., Carciofi, A. C., et al. 2012, A&A, 540, 12
 Stone, R. C. 1991, AJ, 102, 333
 Suh, K.-W. 2004, Journal of The Korean Astronomical Society, 37, 289
 Tauris, T. M. & Takens, R. J. 1998, A&A, 330, 1047
 Tetzlaff, N., Neuhäuser, R., & Hohle, M. M. 2010, MNRAS, 410, 190
 Toalá, J. A., Guerrero, M. A., Ramos-Larios, G., & Guzmán, V. 2015, A&A, 578, A66
 Tout, C. A. 2012, in Proceedings of the International Astronomical Union, ed. M. Richards & I. Hubeny, Vol. 282, 417–424
 Tylenda, R., Hajduk, M., Kamiński, T., et al. 2011, A&A, 528, 10
 van Buren, D., & McCray, R. 1988, ApJ, 329, L93
 van Buren, D., Noriega-Crespo, A., & Dgani, R. 1995, AJ, 110, 2914
 van den Heuvel, E. P. J. & Rappaport, S. 1987, in Physics of Be stars; Proceedings of the Ninety-second IAU Colloquium, Boulder, CO, ed. A. Slettebak & T. P. Snow, 291–307
 van Leeuwen, F. 2007, A&A, 474, 653
 Vanbeveren, D. & Mennekens, N. 2017, in The B[e] Phenomenon: Forty Years of Studies, ed. A. Miroshnichenko, S. Zharikov, D. Korčáková, & M. Wolf (Astronomical Society of the Pacific), 121
 Wang, L., Gies, D. R., & Peters, G. J. 2018, ApJ, 853, 10
 Wegner, W. 2006, MNRAS, 371, 185
 Weis, K. 2003, A&A, 408, 205
 Wellstein, S. & Langer, N. 1999, A&A, 350, 148
 Wellstein, S., Langer, N., & Braun, H. 2001, A&A, 369, 939
 Wenger, M., Oberto, A., Bonnarel, F., et al. 2007, in Astronomical Society of the Pacific Conference Series, ed. S. Ricketts, C. Birdie, & E. Isaksson, 197
 Williams, J. P. & Cieza, L. A. 2011, ARAA, 49, 67
 Wood, P. R., Olivier, E. A., & Kawaler, S. D. 2004, ApJ, 604, 800
 Wright, E. L., Eisenhardt, P. R. M., Mainzer, A. K., et al. 2010, AJ, 140, 1868
 Yoon, S.-C., Woosley, S. E., & Langer, N. 2010, ApJ, 725, 940
 Zahn, J. P. 1975, A&A, 41, 329
 Zhang, F., Li, X. D., & Wang, Z. R. 2003, ApJ, 603, 663
 Zorec, J. & Briot, D. 1997, A&A, 318, 443

Appendix A: Physical extent of bow shocks and centered nebulae

We compare the apex distances of bow shocks in pc with the radii of centered nebulae in pc calculated from their physical size (see Tab. B.2), assuming that all centered nebulae are circular. We carry out a Kuiper test in order to investigate whether the underlying distributions are similar or significantly different from each other. We find that the probability that the two distributions are similar is 5%, that is, 2σ .

Appendix B: Database

Table B.1. Compilation of all parameter values from the literature. In the first column we list the identifier of the star, taken from the BSC, while the second and third columns give the stellar coordinates from SIMBAD. The column 'HD' corresponds to the HD number, while the column 'V' is the apparent V-band magnitude, also taken from SIMBAD. In the column 'spectype', we provide the spectral classification listed in SIMBAD. Parallaxes p with their uncertainties Δp (columns 7 and 8) and proper motions μ_{Ra} with uncertainties $\Delta\mu_{Ra}$ and μ_{Dec} with uncertainties $\Delta\mu_{Dec}$ (columns 9 to 12) are taken from the Hipparcos catalogue (van Leeuwen 2007) if available. Proper motions were converted to the rest frame of the local ISM by correcting for the Galactic rotation following Comerón & Pasquali (2007). Radial velocities RV and uncertainties ΔRV (columns 13 and 14) are mainly taken from Gontcharov (2006). For stars that are not included in this catalogue, we took radial velocities from Kharchenko et al. (2007) or Pourbaix et al. (2004), indicated by the year in the column 'ref'.

Identifier	RA [J2000]	DEC [J2000]	HD	V [mag]	spectype	p [mas]	Δp [mas]	μ_{Ra} [mas yr $^{-1}$]	$\Delta\mu_{Ra}$ [mas yr $^{-1}$]	μ_{Dec} [mas yr $^{-1}$]	$\Delta\mu_{Dec}$ [mas yr $^{-1}$]	RV [km s $^{-1}$]	ΔRV [km s $^{-1}$]	ref
HR 38	00 12 50.25	+37 41 37.2	829	6.7	B3III	1.80	0.42	1.76	0.46	-2.65	0.30	-5.5	2.4	
HD 1976	00 24 15.66	+52 01 11.7	1976	5.6	B5IV	3.26	0.63	13.62	0.43	-3.92	0.33	-15.8	2.3	
HD 2626	00 30 19.93	+59 58 39.2	2626	5.9	B7IV	4.24	0.50	16.26	0.45	-3.29	0.38	-17.4	0.9	
lam Cas	00 31 46.36	+54 31 20.2	2772	4.8	B8Vn	8.64	0.43	41.20	0.29	-16.54	0.35	-12.2	1.3	2007
kap Cas	00 32 59.99	+62 55 54.4	2905	4.2	B1Ia	0.73	0.17	3.65	0.17	-2.07	0.16	0.3	0.8	
53 Psc	00 36 47.31	+15 13 54.2	3379	5.9	B2.5IV	3.14	0.30	0.85	0.29	-13.68	0.23	-8.0	0.9	
zet Cas	00 36 58.28	+53 53 48.9	3360	3.7	B2IV	5.50	0.16	17.38	0.13	-9.86	0.11	-0.2	0.1	
ksi Cas	00 42 04.00	+50 30 45.1	3901	4.8	B2V	2.28	0.51	12.24	0.38	-6.58	0.32	-10.6	7.4	2007
HR 241	00 51 33.79	+51 34 17.1	4881	6.2	B9.5V	3.26	0.36	-3.59	0.30	-10.45	0.24	-13.7	2.9	
gam Cas	00 56 42.53	+60 43 00.3	5394	2.4	B0.5IVpe	5.32	0.56	25.65	0.48	-3.82	0.37	-4.8	1.9	
HR 287	01 02 18.47	+51 02 05.8	6028	6.5	A3V	4.42	0.56	-4.08	0.38	-12.49	0.28	6.4	2.9	
tau And	01 40 34.82	+40 34 37.4	10205	4.9	B5III	4.58	0.25	15.99	0.20	-23.76	0.16	-13.9	2.6	
HR 482	01 42 17.70	+58 37 39.9	10293	6.3	B7III	1.67	0.54	14.15	0.57	-8.19	0.44	-1.0	1.9	
phi Per	01 43 39.64	+50 41 19.4	10516	4.1	B1.5V:e-shell	4.54	0.20	24.59	0.14	14.01	0.13	-4.0	2.1	
1 Per	01 51 59.32	+55 08 50.6	11241	5.5	B1.5V	2.52	0.33	12.05	0.25	-9.18	0.28	-5.4	2.0	2007
g Per	02 02 18.11	+54 29 15.1	12303	5.0	B8III	4.48	0.23	34.32	0.21	-3.27	0.18	-2.3	3.1	
35 Ari	02 43 27.11	+27 42 25.7	16908	4.7	B3V	9.51	0.85	2.06	1.03	-10.37	0.53	13.0	10.0	2007
pi. Cet	02 44 07.35	-13 51 31.3	17081	4.2	B7IV	8.30	0.21	-8.62	0.25	-9.07	0.20	14.3	0.4	
HD 18537	03 00 52.21	+52 21 06.2	18537	5.2	B7V	7.11	1.16	30.21	1.14	-28.38	1.17	-4.3	1.7	
HD 18538	03 00 53.52	+52 21 07.3	18538	6.7	B9V	9.29	1.38	30.18	1.26	-28.29	1.30	-4.3	1.7	
53 Ari	03 07 25.67	+17 52 48.0	19374	6.1	B1.5V	3.92	0.79	-24.32	1.07	7.46	0.70	21.7	1.5	
55 Ari	03 09 36.74	+29 04 37.5	19548	5.7	B8III	3.09	0.49	22.72	0.38	-12.43	0.34	-2.0	4.3	
HR 950	03 12 09.56	+42 22 33.2	19736	6.1	B5V	4.99	0.40	16.95	0.37	-19.25	0.34	5.6	2.9	
HD 20041	03 15 47.97	+57 08 26.2	20041	5.8	A0Ia	1.14	0.42	-1.02	0.49	-3.01	0.38	-11.9	2.9	
29 Per	03 18 37.74	+50 13 19.8	20365	5.2	B3V	5.12	0.29	22.41	0.25	-24.58	0.27	-1.5	0.9	
HD 20336	03 19 59.27	+65 39 08.3	20336	4.8	B2.5Vn(e)	4.28	0.48	11.25	0.33	-14.56	0.50	-3.4	3.5	
HD 21291	03 29 04.13	+59 56 25.2	21291	4.2	B9Ia	1.68	0.50	-2.24	0.40	-0.90	0.39	-5.1	0.4	
HD 21389	03 29 54.74	+58 52 43.5	21389	4.5	A0Ia	1.30	0.56	-1.79	0.49	-1.09	0.52	-6.2	0.4	
HR 1092	03 30 51.71	-66 29 23.0	22252	5.8	B8IV	3.76	0.18	16.98	0.18	1.42	0.23	11.7	4.0	
HR 1074	03 32 40.02	+35 27 42.2	21856	5.9	B1V	1.48	0.34	-8.28	0.42	3.44	0.34	28.1	2.1	
o Per	03 42 22.65	+33 57 54.1	22951	5.0	B0.5V	3.09	0.21	2.71	0.28	-5.91	0.21	22.0	1.5	
del Per	03 42 55.50	+47 47 15.2	22928	3.0	B5III	6.32	0.47	25.58	0.43	-43.06	0.38	4.0	3.7	2007
17 Tau	03 44 52.54	+24 06 48.0	23302	3.7	B6IIIe	8.06	0.25	20.84	0.28	-46.06	0.23	6.7	1.4	
18 Tau	03 45 09.74	+24 50 21.3	23324	5.6	B8V	7.97	0.37	20.36	0.45	-46.52	0.41	4.8	0.8	
20 Tau	03 45 49.61	+24 22 03.9	23408	3.9	B8III	8.51	0.28	20.95	0.31	-45.98	0.28	7.4	0.5	
eta Tau	03 47 29.08	+24 06 18.5	23630	2.9	B7III	8.09	0.42	19.34	0.39	-43.67	0.33	5.4	1.2	
HD 23625	03 47 52.67	+33 35 59.5	23625	6.7	B3V+B8.5V	3.07	0.82	4.16	0.92	-5.16	0.84	20.0	2.0	2007
e Tau	03 48 16.27	+11 08 35.9	23793	5.1	B3V	7.19	0.76	26.00	0.71	-28.84	0.57	16.2	0.1	
27 Tau	03 49 09.74	+24 03 12.3	23850	3.6	B8III	8.53	0.39	17.70	0.36	-44.18	0.32	-0.4	10.0	2007
HD 24131	03 51 53.72	+34 21 32.8	24131	5.8	B1V	3.87	0.36	5.62	0.43	-3.65	0.38	20.6	0.7	
31 Tau	03 52 00.23	+06 32 05.7	24263	5.8	B5V	4.19	0.93	9.25	1.32	-3.59	1.25	15.7	1.8	2007
eps Per	03 57 51.23	+40 00 36.8	24760	2.9	B1.5III	5.11	0.23	14.06	0.26	-23.78	0.17	-0.5	1.1	
ksi Per	03 58 57.90	+35 47 27.7	24912	4.1	O7.5III(n)(f)	2.62	0.51	3.62	0.61	1.74	0.50	65.4	0.8	
lam Tau	04 00 40.82	+12 29 25.2	25204	3.4	B4IV	6.74	0.17	-8.02	0.24	-14.42	0.16	13.4	4.0	
35 Eri	04 01 32.05	-01 32 58.8	25340	5.3	B5III/IV	7.88	0.27	27.74	0.36	-14.69	0.34	15.7	0.8	
40 Tau	04 03 44.61	+05 26 08.2	25558	5.3	B5V	5.09	0.32	2.18	0.48	-5.56	0.41	13.0	0.8	
lam Per	04 06 35.04	+50 21 04.6	25642	4.3	A0IVn	7.73	0.22	-12.75	0.19	-35.60	0.16	6.1	2.7	
41 Tau	04 06 36.41	+27 35 59.6	25823	5.2	Ap	7.76	0.36	21.88	0.39	-52.34	0.33	2.3	4.2	

Table B.1. continued.

Identifier	RA [J2000]	DEC [J2000]	HD	V [mag]	spectype	p [mas]	Δp [mas]	μ_{RA} [mas yr $^{-1}$]	$\Delta\mu_{RA}$ [mas yr $^{-1}$]	μ_{DEC} [mas yr $^{-1}$]	$\Delta\mu_{DEC}$ [mas yr $^{-1}$]	RV [km s $^{-1}$]	ΔRV [km s $^{-1}$]	ref
HR 1307	04 13 34.57	+10 12 44.8	26676	6.2	B8V	7.56	0.81	21.49	1.42	-25.44	1.05	7.6	0.8	2007
mu. Tau	04 15 32.06	+08 53 32.5	26912	4.3	B3IV	7.16	0.34	19.46	0.34	-22.11	0.29	16.3	0.6	
HD 27192	04 20 11.51	+50 55 15.4	27192	5.5	B1.5IV	3.01	0.38	1.19	0.39	-7.52	0.33	-17.8	2.7	
d Per	04 21 33.17	+46 29 56.0	27396	4.8	B4IV	6.43	0.28	20.06	0.29	-35.45	0.23	7.3	0.9	
72 Tau	04 27 17.45	+22 59 46.8	28149	5.5	B7V	8.63	0.34	-0.71	0.37	-14.46	0.35	7.3	2.6	
HR 1415	04 28 32.12	+01 22 51.0	28375	5.5	B5III/IV	8.52	0.35	17.81	0.42	-21.50	0.47	18.0	4.3	
del Cae	04 30 50.10	-44 57 13.5	28873	5.1	B2IV/V	4.63	0.19	1.64	0.21	-3.09	0.23	14.2	0.8	
alf Cam	04 54 03.01	+66 20 33.6	30614	4.3	O9Ia	0.52	0.19	-0.13	0.14	6.89	0.15	13.0	10.0	2007
HR 1640	05 03 52.12	-14 22 12.8	32612	6.4	B2IV	1.76	0.41	1.65	0.34	3.02	0.32	16.0	4.3	
11 Cam	05 06 08.45	+58 58 20.5	32343	5.1	B3Ve	4.76	0.31	-7.31	0.26	-7.85	0.22	-11.0	0.8	
105 Tau	05 07 55.44	+21 42 17.4	32991	5.9	B2Ve	3.02	0.44	2.56	0.51	-5.08	0.29	16.4	1.0	
lam Eri	05 09 08.78	-08 45 14.7	33328	4.3	B2IVne	4.02	0.18	0.25	0.16	-1.97	0.11	2.0	4.2	
HD 34078	05 16 18.15	+34 18 44.3	34078	6.0	O9.5V	1.74	0.72	-3.58	0.72	43.73	0.39	56.7	0.6	2007
tau Ori	05 17 36.39	-06 50 39.9	34503	3.6	B5III	6.60	0.15	-17.61	0.16	-9.24	0.11	20.1	2.7	
15 Cam	05 19 27.86	+58 07 02.5	34233	6.1	B5V	4.15	0.54	6.78	0.49	-17.02	0.40	6.7	3.7	2007
HR 1763	05 21 43.56	+08 25 42.8	34989	5.8	B1V	2.29	0.36	-1.46	0.44	-2.37	0.32	25.3	3.5	
115 Tau	05 27 10.09	+17 57 44.0	35671	5.4	B5V	5.94	0.34	7.70	0.40	-20.54	0.21	14.9	0.9	
o Tau	05 27 38.08	+21 56 13.1	35708	4.9	B2.5V	5.22	0.21	0.05	0.24	-7.06	0.12	16.5	0.1	
ups Ori	05 31 55.86	-07 18 05.5	36512	4.6	O9.7V	1.14	0.25	-0.10	0.18	-4.87	0.14	17.1	2.5	
HR 1847	05 32 14.14	+17 03 29.2	36408	6.1	B7III	1.09	2.04	-4.01	2.63	-11.79	1.34	15.0	4.3	
HR 1861	05 32 41.35	-01 35 30.6	36591	5.3	B2II/III	2.09	0.80	-1.95	0.67	0.80	0.40	34.3	0.7	2007
VV Ori	05 33 31.45	-01 09 21.9	36695	5.3	B9IV/V	2.22	0.35	-0.82	0.33	-1.07	0.18	3.3	10.0	2007
120 Tau	05 33 31.63	+18 32 24.8	36576	5.7	B2IV-Ve	2.10	0.32	2.78	0.41	-0.05	0.14	41.0	4.0	
phi01 Ori	05 34 49.24	+09 29 22.5	36822	4.4	B0III	3.00	0.25	0.27	0.29	-2.26	0.12	33.2	10.0	2007
c Ori	05 35 23.16	-04 50 18.1	37018	4.6	B1V	3.69	1.20	4.52	1.08	-7.11	0.66	28.4	3.4	
121 Tau	05 35 27.13	+24 02 22.5	36819	5.4	B2.5IV	5.90	0.22	15.52	0.31	-19.67	0.12	16.8	0.9	
sig Ori	05 38 44.78	-02 36 00.1	37468	3.8	O9.5V	3.04	8.92	22.63	10.83	13.45	5.09	29.9	1.6	2007
ome Ori	05 39 11.14	+04 07 17.3	37490	4.6	B3Ve	2.36	0.29	0.84	0.28	0.00	0.16	20.5	0.9	
125 Tau	05 39 44.20	+25 53 49.5	37438	5.2	B3IV	7.63	0.33	11.04	0.36	-23.59	0.20	16.5	1.9	
133 Tau	05 47 42.91	+13 53 58.6	38622	5.3	B2IV-V	5.15	0.36	4.97	0.36	-12.95	0.25	26.2	0.7	
HR 2058	05 54 34.70	-04 03 53.0	39777	6.5	B2III/IV	2.60	0.49	2.75	0.54	-1.15	0.41	25.9	2.7	
139 Tau	05 57 59.66	+25 57 14.1	40111	4.8	B0/II/III	2.10	0.19	-2.06	0.26	-1.95	0.11	8.0	4.2	
HD 41335	06 04 13.50	-06 42 32.2	41335	5.2	B3/5Vnne	2.48	0.75	-3.70	0.74	4.98	0.71	24.1	7.4	2007
nu Ori	06 07 34.33	+14 46 06.5	41753	4.4	B3V	6.32	0.33	6.78	0.34	-20.23	0.21	24.1	2.7	
del Pic	06 10 17.91	-54 58 07.1	42933	4.8	B1/2(III)n	2.51	0.15	-4.90	0.14	7.41	0.17	30.6	2.8	
HD 43955	06 18 13.73	-19 58 01.1	43955	5.5	B2/3V	4.10	0.28	-5.74	0.22	7.06	0.22	17.9	2.3	
HR 2276	06 20 52.12	+11 45 22.4	44173	6.6	B5III	1.10	0.53	-4.17	0.55	-4.13	0.40	18.8	3.0	
bet CMa	06 22 41.99	-17 57 21.3	44743	2.0	B1II-III	6.62	0.22	-3.23	0.19	-0.78	0.20	33.7	0.5	
10 Mon	06 27 57.57	-04 45 43.8	45546	5.0	B2V	3.00	0.24	-5.78	0.21	-2.86	0.19	25.3	0.8	
HD 47432	06 38 38.19	+01 36 48.7	47432	6.3	O9.7Ib	1.50	0.54	-0.34	0.62	-0.83	0.42	60.1	1.5	
psi03 Aur	06 38 49.18	+39 54 09.2	47100	5.3	B8III	2.38	0.39	-8.68	0.46	-11.61	0.29	9.0	4.2	
HD 48099	06 41 59.23	+06 20 43.5	48099	6.4	O5V((f))z+O9:	1.17	0.41	0.84	0.41	2.55	0.31	28.6	2.8	
HD 49662	06 48 57.74	-15 08 41.0	49662	5.4	B7IV	6.17	0.75	-2.72	0.77	-4.66	0.78	23.0	7.4	2007
iot CMa	06 56 08.22	-17 03 15.3	51309	4.4	B3Ib/II	1.30	0.20	-3.56	0.17	2.42	0.20	41.2	1.6	
gam CMa	07 03 45.49	-15 37 59.8	53244	4.1	B8II	7.38	0.21	-0.14	0.19	-11.36	0.21	32.0	7.4	2007
V* FN CMa	07 06 40.77	-11 17 38.4	53974	5.4	B0IIIIn	1.07	0.61	-3.14	0.72	3.32	0.55	31.0	4.2	
A Pup	07 08 51.07	-39 39 20.4	54893	4.8	B3IV/V	4.48	0.14	-10.69	0.12	7.71	0.17	19.5	2.8	
HD 54662	07 09 20.25	-10 20 47.6	54662	6.2	O7Vzvar?	1.58	0.45	-1.96	0.52	4.40	0.37	57.9	2.5	
26 CMa	07 12 12.21	-25 56 33.3	55522	5.9	B2IV/V	3.89	0.41	-5.55	0.21	7.86	0.34	21.6	2.9	
HD 55857	07 13 36.45	-27 21 22.9	55857	6.1	B2II	0.96	0.42	-3.87	0.29	6.43	0.35	33.0	2.3	
HR 2769	07 16 31.85	-38 19 08.1	56733	5.8	B4V	5.34	0.27	-7.78	0.19	4.89	0.28	32.0	7.2	2007
HD 57682	07 22 02.05	-08 58 45.8	57682	6.4	O9.2IV			10.46	0.45	13.38	0.34	24.1	1.2	
HR 2812	07 22 13.53	-19 00 59.8	57821	5.0	B5II/III	6.78	0.26	-1.69	0.19	-6.91	0.25	32.9	1.6	
z Pup	07 33 51.04	-36 20 18.2	60606	5.4	B2Vne	2.75	0.24	-7.94	0.19	4.00	0.21	-9.0	7.4	2007

Table B.1. continued.

Identifier	RA [J2000]	DEC [J2000]	HD	V [mag]	spectype	p [mas]	Δp [mas]	μ_{RA} [mas yr $^{-1}$]	$\Delta\mu_{RA}$ [mas yr $^{-1}$]	μ_{DEC} [mas yr $^{-1}$]	$\Delta\mu_{DEC}$ [mas yr $^{-1}$]	RV [km s $^{-1}$]	ΔRV [km s $^{-1}$]	ref
e Pup	07 38 43.90	-36 29 48.6	61641	5.8	B3III	3.27	0.26	-7.23	0.21	4.63	0.23	19.0	4.3	
HD 61831	07 39 27.34	-38 18 28.9	61831	4.8	B3V	5.87	0.16	-21.11	0.14	15.81	0.14	26.4	2.8	
HR 3023	07 47 12.55	-22 31 10.2	63271	5.9	B1/2V	1.99	0.33	-7.80	0.26	9.92	0.24	7.0	4.3	
V* V372 Car	07 52 29.74	-54 22 01.8	64722	5.7	B2IV	2.44	0.20	-4.17	0.22	8.03	0.20	18.0	4.3	
HR 3091	07 54 11.01	-35 52 38.2	64802	5.5	B2V	4.81	0.23	-2.77	0.17	3.66	0.21	27.7	2.8	
V* V Pup	07 58 14.44	-49 14 41.7	65818	4.4	B1Vp+B2:	3.40	0.29	-5.34	0.27	7.12	0.24	16.0	4.1	
HD 66005	07 59 12.31	-49 58 36.8	66005	6.2		B2/3		0.94	6.06	-2.89	4.90	13.0	7.4	2007
HD 66006	07 59 13.57	-49 58 25.6	66006	6.3	B2/3			0.41	4.66	0.13	3.45	23.0	7.4	2007
HR 3159	08 00 19.97	-63 34 02.8	66591	4.8	B4V	6.53	0.13	-1.89	0.15	19.21	0.14	22.1	2.8	
HR 3156	08 00 49.94	-54 09 04.6	66441	5.8	B5Vn	4.25	0.25	-25.42	0.30	8.74	0.20	0.0	3.7	2007
V* V461 Car	08 01 23.04	-54 30 55.9	66546	6.1	B2IV	2.42	0.25	-5.23	0.30	5.99	0.23	34.0	7.4	2007
eps Vol	08 07 55.79	-68 37 01.4	68520	4.4	B5III	5.80	0.39	-29.14	0.41	29.26	0.43	9.0	0.3	
16 Pup	08 09 01.64	-19 14 42.1	67797	4.4	B5V	7.01	0.22	-9.87	0.18	-5.55	0.21	19.9	1.2	
HD 68895	08 12 30.79	-46 15 51.4	68895	6.0	B5V	3.12	0.44	-3.92	0.56	9.06	0.32	12.7	1.8	2007
V* NO Vel	08 13 36.15	-46 59 29.9	69144	5.1	B3III	2.40	0.20	-10.11	0.20	9.88	0.17	25.0	4.5	
HD 71510C	08 25 31.10	-51 43 40.0	71510	10.8	G3V	4.69	0.22	-14.31	0.24	17.08	0.20	18.0	4.2	
HR 3358	08 29 04.75	-47 55 44.1	72108	5.3	B1.5V+B4V	1.53	0.34	-6.90	0.43	7.12	0.34	29.0	3.7	2007
d Car	08 40 37.03	-59 45 39.6	74375	4.3		B2III	2.26	0.11	-6.63	0.12	5.32	0.12	12.9	0.7
eta Hya	08 43 13.47	+03 23 55.2	74280	4.3	B3V	5.56	0.24	-19.39	0.27	-1.08	0.20	16.1	0.3	
HR 3479	08 44 51.93	-37 08 50.1	74824	5.7	B3III	2.06	0.27	-8.47	0.17	4.42	0.20	12.0	10.0	2007
HR 3503	08 48 00.22	-52 51 00.5	75466	6.3	B8V	7.05	0.24	-25.13	0.26	23.31	0.26	11.6	1.5	
f Vel	08 50 33.46	-46 31 45.1	75821	5.1	B1Ib	1.00	0.27	-3.69	0.28	3.36	0.28	27.2	0.2	2007
HD 77002	08 56 58.42	-59 13 45.6	77002	4.9	B2V	4.84	0.21	-8.26	0.20	8.04	0.21	26.8	2.8	
E Car	09 05 38.38	-70 32 18.6	78764	4.7	B2(IV)n	3.37	0.38	-4.11	0.44	8.87	0.37	19.0	7.4	2007
a Car	09 10 58.09	-58 58 00.8	79351	3.4		B2IV-V	7.30	0.35	-16.64	0.33	15.00	0.35	23.3	4.0
HR 3784	09 30 05.11	-51 31 01.8	82419	5.5	B8III	7.54	0.20	-19.29	0.17	12.04	0.18	10.0	4.2	
zet Cha	09 33 53.38	-80 56 28.5	83979	5.1	B4IV	5.70	0.15	-34.91	0.17	14.18	0.16	-42.0	4.2	
kap Hya	09 40 18.36	-14 19 56.3	83754	5.1	B3/5IV/V	7.48	0.30	-23.41	0.41	-21.10	0.22	20.6	2.0	
HR 3878	09 45 22.01	-30 12 09.9	84567	6.5		B0IV	0.93	0.36	-11.44	0.26	5.92	0.30	31.7	3.0
HR 3886	09 46 30.37	-44 45 18.2	84816	5.5	B2V	3.27	0.41	-13.34	0.32	-0.78	0.31	-4.0	7.4	2007
HR 3920	09 53 00.09	-55 22 23.5	85817	6.5	B1IIIIn	1.23	0.27	-11.84	0.24	4.08	0.23	-18.0	7.4	2007
HD 85980	09 54 17.65	-45 17 00.7	85980	5.8		B5V	3.27	0.40	-16.57	0.35	4.92	0.36	13.0	4.3
tet Car	10 42 57.40	-64 23 40.0	93030	2.8	B0Vp	7.16	0.21	-18.36	0.23	12.03	0.18	20.0	1.0	2004
HR 4222	10 46 51.22	-64 23 00.5	93607	4.8	B4V	6.79	0.17	-17.96	0.19	9.65	0.15	16.0	4.2	
HD 96706	11 06 49.89	-70 52 40.5	96706	5.6	B3IV/V	3.96	0.22	-22.35	0.23	3.36	0.19	7.4	4.3	
pi. Cen	11 21 00.44	-54 29 27.9	98718	3.9		B5Vn	9.12	0.34	-35.85	0.34	-1.72	0.27	9.4	3.7
HD 99104	11 23 21.40	-64 57 17.0	99103	5.1	B5IV	8.08	0.38	-22.60	0.39	7.03	0.36	19.3	2.8	
HR 4403	11 24 22.05	-42 40 08.8	99171	6.1	B2V	1.18	0.57	-9.20	0.32	0.57	0.34	9.7	1.5	
HD 105521	12 08 54.59	-41 13 53.8	105521	5.5	B3IVe	2.05	0.25	-11.51	0.23	-7.76	0.17	0.0	3.7	2007
del Cru	12 15 08.72	-58 44 56.1	106490	2.8	B2IV	9.45	0.15	-35.81	0.12	-10.36	0.12	22.2	2.6	
G Cen	12 26 31.76	-51 27 02.3	108257	4.8	B3V(n)	7.28	0.24	-30.66	0.18	-10.13	0.14	5.0	4.2	
alf Cru	12 26 35.90	-63 05 56.7	108248	0.8		B0.5IV+B1V	10.13	0.50	-35.83	0.47	-14.86	0.43	11.9	2.4
sig Cen	12 28 02.38	-50 13 50.3	108483	3.9	B2V	7.92	0.18	-32.36	0.15	-12.51	0.13	8.0	4.1	
alf Mus	12 37 11.02	-69 08 08.0	109668	2.6	B2IV	10.34	0.11	-40.20	0.10	-12.80	0.10	13.0	4.0	
bet Mus	12 46 16.80	-68 06 29.2	110879	3.1	B2V	9.55	0.41	-41.97	0.43	-8.89	0.31	42.0	7.4	2007
HD 110956	12 46 22.71	-56 29 19.7	110956	4.6	B2/3V	8.48	0.22	-33.03	0.14	-14.84	0.13	16.6	2.8	
bet Cru	12 47 43.26	-59 41 19.8	111123	1.2	B1IV	11.71	0.98	-42.97	0.72	-16.18	0.68	15.6	0.4	
mu.01 Cru	12 54 35.62	-57 10 40.5	112092	4.0	B2IV-V	7.87	0.17	-30.69	0.13	-13.08	0.11	13.9	0.7	
mu.02 Cru	12 54 36.89	-57 10 07.2	112092	5.2	B5Vne	8.01	0.29	-32.49	0.23	-10.92	0.19	13.9	0.7	
Ksi02 Cen	13 06 54.64	-49 54 22.5	113791	4.3	B3V	6.98	0.24	-26.15	0.23	-12.03	0.15	14.3	4.1	
HR 5027	13 20 48.34	-55 48 02.5	115842	6.1	B0.5Ia/ab	0.65	0.44	-3.04	0.31	3.93	0.36	-3.0	4.3	
HR 5140	13 42 01.09	-58 47 13.5	118978	5.4		B9III	4.17	0.57	-31.75	0.55	-11.63	0.48	-8.0	7.4
nu Cen	13 49 30.28	-41 41 15.8	120307	3.4	B2IV	7.47	0.17	-26.77	0.12	-20.18	0.08	8.0	2.0	
47 Hya	13 58 31.15	-24 58 20.1	121847	5.2	B8V	9.80	0.19	-49.36	0.21	-29.53	0.15	5.0	4.2	

Table B.1. continued.

Identifier	RA [J2000]	DEC [J2000]	HD	V [mag]	spectype	p [mas]	Δp [mas]	μ_{RA} [mas yr $^{-1}$]	$\Delta\mu_{RA}$ [mas yr $^{-1}$]	μ_{DEC} [mas yr $^{-1}$]	$\Delta\mu_{DEC}$ [mas yr $^{-1}$]	RV [km s $^{-1}$]	ΔRV [km s $^{-1}$]	ref
eps Aps	14 22 23.16	-80 06 32.2	124771	5.1	B3V	5.06	0.22	-9.51	0.20	-14.34	0.21	4.5	4.2	
V* HX Lup	14 22 38.71	-48 19 11.5	125721	6.1	B2II/III	1.49	0.58	-5.58	0.43	-5.97	0.57	-18.0	4.3	
tau01 Lup	14 26 08.22	-45 13 17.1	126341	4.6	B2IV	2.99	0.21	-13.09	0.22	-14.67	0.18	-21.5	2.8	
sig Lup	14 32 37.06	-50 27 25.8	127381	4.4	B1/B2V	5.67	0.19	-29.26	0.16	-15.72	0.16	-1.5	2.7	
bet Lib	15 17 00.41	-09 22 58.5	135742	2.6	B8Vn	17.62	0.16	-98.10	0.18	-19.65	0.15	-35.6	1.8	
b Sco	15 50 58.74	-25 45 04.7	141637	4.6	B1.5Vn	6.59	0.27	-14.20	0.33	-25.12	0.26	-3.0	4.7	
lam Lib	15 53 20.05	-20 10 01.4	142096	5.0	B3V	10.54	0.91	-9.81	1.35	-26.85	1.00	-11.5	2.2	
2 Sco	15 53 36.72	-25 19 37.7	142114	4.6	B2.5Vn	6.49	0.51	-15.12	0.62	-25.18	0.56	-9.3	1.6	
HR 5906	15 53 53.92	-24 31 59.4	142165	5.4	B5V	7.76	0.52	-12.59	0.67	-25.49	0.64	-6.3	10.0	2007
3 Sco	15 54 39.53	-25 14 37.5	142301	5.9	B8III/IV	6.33	0.43	-13.16	0.60	-25.55	0.46	-8.7	4.3	
rho Sco	15 56 53.08	-29 12 50.7	142669	3.9	B2IV-V	6.91	0.19	-15.68	0.21	-24.88	0.19	3.3	10.0	2007
48 Lib	15 58 11.37	-14 16 45.7	142983	4.9	B8Ia/Iab	6.97	0.24	-12.44	0.25	-16.73	0.21	-7.5	1.8	
pi. Sco	15 58 51.11	-26 06 50.8	143018	2.9	B1V+B2:V:	5.57	0.64	-11.42	0.78	-26.83	0.74	-7.4	1.3	
del Sco	16 00 20.01	-22 37 18.1	143275	2.3	B0.3IV	6.64	0.89	-10.21	1.01	-35.41	0.71	-6.0	0.5	2004
ome Sco	16 06 48.43	-20 40 09.1	144470	4.0	B1V	6.92	0.26	-8.98	0.23	-23.48	0.16	-4.4	3.0	
11 Sco	16 07 36.42	-12 44 43.5	144708	5.8	B9V	8.90	0.60	-42.16	0.61	-25.86	0.55	-25.0	7.4	2007
HR 6026	16 11 58.60	-19 27 00.2	145501	6.3	B8/9V			-4.20		-18.00				
nu Sco	16 11 59.74	-19 27 38.5	145502	4.0	B2V	6.88	0.76	-7.65	0.71	-23.71	0.47	4.1	10.0	2007
13 Sco	16 12 18.20	-27 55 34.9	145482	4.6	B2V	6.81	0.16	-10.38	0.18	-23.94	0.14	-3.8	7.4	2007
HR 6054	16 14 53.43	-25 28 37.1	146001	6.0	B8V	6.72	0.40	-9.41	0.37	-21.73	0.31	-8.4	2.7	
sig Sco	16 21 11.32	-25 35 34.1	147165	2.9	O9.5(V)+B7(V)	4.68	0.60	-10.60	0.78	-16.28	0.43	2.5	2.0	
i Sco	16 30 12.48	-25 06 54.8	148605	4.8	B3V	7.89	0.24	-4.45	0.23	-26.33	0.23	0.0	5.9	2007
N Sco	16 31 22.93	-34 42 15.7	148703	4.2	B2III-IV	5.88	0.19	-12.05	0.20	-18.16	0.13	0.8	1.5	
tau Sco	16 35 52.96	-28 12 57.7	149438	2.8	B0.2V	6.88	0.53	-9.89	0.61	-22.83	0.55	1.7	0.9	
zet Oph	16 37 09.54	-10 34 01.5	149757	2.6	O9.2IVnn	8.91	0.20	15.26	0.26	24.79	0.22	-9.0	5.5	2007
HR 6219	16 47 19.66	-58 20 29.2	150898	5.6	B0Ia/ab	1.21	0.31	-4.64	0.24	-20.28	0.23	-53.3	2.9	
HR 6387	17 12 25.06	-27 45 43.6	155401	6.1	B9V(n)	6.50	0.40	-6.76	0.35	-48.62	0.20	1.0	10.0	2007
V* U Oph	17 16 31.72	+01 12 38.0	156247	5.9	B3V	4.99	0.41	-3.46	0.39	-15.94	0.22	-10.8	2.9	
tet Oph	17 22 00.58	-24 59 58.3	157056	3.3	OB	7.48	0.17	-7.37	0.18	-23.94	0.10	-2.1	3.6	2007
HR 6523	17 33 07.39	-41 10 23.0	158799	5.8	B9III	2.15	0.42	4.03	0.50	-3.38	0.32	-19.1	3.2	
kap Sco	17 42 29.28	-39 01 47.9	160578	2.4	B1.5III	6.75	0.17	-6.05	0.21	-25.54	0.13	-14.0	2.8	
HD 161056	17 43 47.02	-07 04 46.6	161056	6.3	B3II/III	3.00	0.54	-4.32	0.47	-10.60	0.29	-26.0	4.3	
iot02 Sco	17 50 11.11	-40 05 25.6	161912	4.8	A2Ib	1.28	0.24	3.90	0.32	-2.42	0.18	-10.2	3.1	
HR 6755	18 06 07.40	-08 19 26.2	165402	5.9	B2II/III	6.30	0.76	-3.76	0.82	-16.57	0.51	-23.0	4.3	
HR 6788	18 10 55.35	-33 48 00.2	166197	6.2	B2II/III			3.18	0.53	0.02	0.28	-25.0	4.3	
HD 166841	18 18 00.96	-68 13 45.3	166841	6.3	B8/9V	5.35	0.42	-0.20	0.33	-17.09	0.32	18.8	1.8	
HD 170580	18 30 05.12	+04 03 55.3	170580	6.7	B2V	1.97	0.37	-0.61	0.41	-6.46	0.35	-22.0	1.0	
HD 172910	18 44 19.36	-35 38 31.2	172910	4.9	B2V	6.99	0.23	-0.68	0.25	-27.24	0.15	3.9	2.8	
HD 173117	18 44 49.60	-25 00 39.3	173117	5.8	B8III	5.64	0.37	1.42	0.49	-22.54	0.26	15.0	7.4	2007
HD 174237	18 46 43.09	+52 59 16.7	174237	5.9	B3+F5III	2.52	0.24	10.65	0.24	-3.37	0.24	-2.1	2.3	
V* V686 CrA	18 56 40.50	-37 20 35.7	175362	5.4	B3V	7.58	0.27	9.05	0.33	-23.62	0.20	1.3	0.8	
HR 7185	18 59 12.29	+39 13 02.4	176582	6.4	B5V	3.42	0.30	-0.45	0.22	-0.67	0.35	-14.0	4.3	
HR 7173	18 59 17.34	+10 08 27.6	176304	6.8	B2Vp	1.51	0.60	1.08	0.55	-3.52	0.46	-14.8	3.0	
HR 7202	19 01 17.36	+26 17 29.1	176871	5.7	B5V	5.02	0.29	-0.66	0.19	-9.28	0.28	-20.4	1.2	
HR 7200	19 01 22.55	+20 49 58.2	176819	6.8	B2IV-V	1.66	0.39	-0.29	0.25	-5.78	0.36	-10.3	4.4	
20 Aql	19 12 40.71	-07 56 22.3	179406	5.3	B2/III	3.33	0.25	14.93	0.23	-6.63	0.16	-23.0	0.7	
21 Aql	19 13 42.70	+02 17 37.3	179761	5.2	B7III	4.59	0.29	6.95	0.25	-3.28	0.20	-3.2	0.1	
1 Vul	19 16 13.04	+21 23 25.5	180554	4.8	B4IV	4.02	0.37	0.21	0.33	-6.84	0.37	-25.2	10.0	2007
HR 7361	19 19 46.14	+64 23 26.9	182308	6.5	A0Ib	3.55	0.27	-0.86	0.29	8.00	0.31	-18.8	0.4	
HR 7471	19 38 48.99	+03 22 53.5	185423	6.4	B5Ib/II			0.54	0.53	-0.11	0.20	-1.0	4.3	
sig Aql	19 39 11.64	+05 23 52.0	185507	5.2	B3V	4.18	0.40	3.97	0.49	-4.26	0.36	-4.5	2.8	
HD 186568	19 43 51.45	+34 09 45.8	186568	6.1	B8III	3.02	0.27	6.78	0.19	4.09	0.32	-8.8	0.1	
HR 7516	19 45 52.23	-02 53 00.4	186660	6.5	B2III/IV	2.76	0.53	-1.08	0.55	-1.77	0.42	-17.4	2.9	
9 Sge	19 52 21.76	+18 40 18.8	188001	6.2	O7.5Iabf			-2.03	0.66	-10.30	0.56	13.6	2.3	

Table B.1. continued.

Article number, page 16 of 21

Identifier	RA [J2000]	DEC [J2000]	HD	V [mag]	spectype	p [mas]	Δp [mas]	μ_{RA} [mas yr $^{-1}$]	$\Delta\mu_{RA}$ [mas yr $^{-1}$]	μ_{DEC} [mas yr $^{-1}$]	$\Delta\mu_{DEC}$ [mas yr $^{-1}$]	RV [km s $^{-1}$]	ΔRV [km s $^{-1}$]	ref
57 Aql A	19 54 37.65	-08 13 38.2	188293	5.7	B7Vn	6.76	0.37	6.61	0.32	-25.75	0.30	-6.0	7.4	2007
57 Aql B	19 54 38.06	-08 14 13.4	188294	6.4	B8V	6.42	0.58	2.13	0.49	-30.77	0.46	-5.0	7.4	2007
HD 190603	20 04 36.17	+32 13 07.0	190603	5.7	B1.5Ia	0.57	0.29	-2.93	0.20	-11.07	0.22	21.1	2.9	
ome01 Cyg	20 30 03.54	+48 57 05.6	195556	4.9	B2.5IV	3.59	0.18	10.63	0.18	7.22	0.16	-21.9	2.0	
28 Vul	20 38 31.91	+24 06 57.4	196740	5.0	B5IV	6.24	0.24	9.34	0.19	-7.92	0.17	-22.6	1.2	
ups Pav	20 41 57.08	-66 45 38.4	196519	5.1	B9III	4.15	0.27	9.15	0.15	-23.79	0.19	7.0	4.2	
V* V379 Cep	20 43 13.68	+57 06 50.3	197770	6.3	B2III	0.31	9.40	-2.36	0.24	-3.54	0.33	-15.0	4.3	
55 Cyg	20 48 56.29	+46 06 50.9	198478	4.9	B4Ia	1.40	0.17	-2.65	0.20	-2.84	0.17	-7.2	2.8	
BW Vul	20 54 22.40	+28 31 19.2	199140	6.5	B2IIIv	3.12	0.40	1.42	0.40	-5.11	0.30	-6.1	3.0	
HD 199478	20 55 49.80	+47 25 03.6	199478	5.6	B8Ia			-2.09	0.22	-3.91	0.25	-15.0	7.4	2007
HR 8105	21 11 03.77	+36 17 58.5	201819	6.5	B1Vp	0.87	0.34	0.37	0.23	0.53	0.30	-6.0	3.0	
HD 202214	21 11 48.24	+59 59 11.8	202214	5.7	O9.5IV	0.76	0.42	-2.39	0.30	-3.17	0.36	-16.2	2.9	
HD 203025	21 17 18.79	+58 36 41.3	203025	6.4	B2IIIe	1.19	0.29	-3.34	0.26	-3.20	0.24	-6.1	7.4	2007
sig Cyg	21 17 24.95	+39 23 40.9	202850	4.2	A0Ia	1.13	0.19	-0.13	0.13	-3.58	0.14	-5.3	0.4	
68 Cyg	21 18 27.19	+43 56 45.4	203064	5.0	O7.5IIIIn((f))	0.70	0.23	4.85	0.22	-8.40	0.20	-30.0	10.0	2007
alf Cep	21 18 34.77	+62 35 08.1	203280	2.5	A8Vn	66.50	0.11	150.55	0.90	49.09	0.09	-15.8	1.1	
6 Cep	21 19 22.22	+64 52 18.7	203467	5.2	B3IVe	1.64	0.17	5.20	0.18	5.69	0.16	-16.5	1.4	
HD 207198	21 44 53.28	+62 27 38.0	207198	5.9	O8.5II	1.09	0.24	-3.24	0.30	-2.29	0.23	-17.6	1.4	
pi.02 Cyg	21 46 47.61	+49 18 34.5	207330	4.2	B3III	2.95	0.34	2.77	0.30	-2.00	0.31	-12.3	7.4	2007
HR 8341	21 49 26.87	+20 27 44.8	207563	6.3	B2V	2.79	0.31	1.17	0.28	-0.06	0.25	-16.3	1.8	
HR 8357	21 52 01.04	+55 47 48.2	208095	5.7	B6IV-V	2.17	2.31	17.25	2.04	-5.73	1.89	-19.4	4.3	
ksi Cep	22 03 47.45	+64 37 40.7	209790	6.5	Am+F7/8V	33.79	1.06	215.46	1.14	91.06	0.97	-10.7	4.1	
lam Cep	22 11 30.58	+59 24 52.2	210839	5.0	O6.5I(n)fp	1.65	0.22	-7.46	0.22	-11.09	0.18	-75.1	0.9	
HR 8490	22 13 49.70	+63 09 44.4	211242	6.1	B8Vn	2.50	0.25	-7.75	0.34	-7.93	0.29	15.1	3.6	
30 Peg	22 20 27.58	+05 47 22.2	211924	5.4	B5IV	2.56	0.30	19.57	0.35	2.63	0.21	-13.8	1.0	
4 Lac	22 24 30.99	+49 28 35.0	212593	4.6	A0Ib	1.45	0.35	-5.55	0.31	-2.85	0.32	-26.0	1.7	
pi. Aqr	22 25 16.62	+01 22 38.6	212571	4.6	B1III-IVe	4.17	0.27	17.83	0.27	2.41	0.20	-4.9	0.1	2004
HD 212883	22 26 45.56	+37 26 37.3	212883	6.5	B2V	2.18	0.62	-0.48	0.67	-5.48	0.54	-9.0	1.0	
26 Cep	22 27 05.31	+65 07 56.2	213087	5.5	B0.5Ib	0.61	0.24	0.10	0.27	-2.62	0.24	-12.7	1.6	
8 Lac B	22 35 52.11	+39 37 41.3	214168	5.7	B1.5Vs	1.51	1.31	9.95	6.63	-11.54	4.92	-11.7	0.9	
10 Lac	22 39 15.68	+39 03 01.0	214680	4.9	O9V	1.89	0.22	-0.32	0.25	-5.46	0.19	-10.1	0.3	
12 Lac	22 41 28.65	+40 13 31.6	214993	5.2	B2III	2.43	0.29	-1.59	0.33	-5.33	0.28	-12.5	2.2	
HD 215191	22 42 55.48	+37 48 10.1	215191	6.4	B1V	3.11	0.46	-0.50	0.48	-5.61	0.36	-17.8	2.9	
HR 8677	22 47 23.24	+58 28 58.9	215907	6.4	B9.5IV	3.24	0.38	7.87	0.38	7.13	0.31	0.3	2.4	2007
14 Lac	22 50 21.77	+41 57 12.2	216200	5.9	B4+F9III	2.87	0.46	7.96	0.25	-3.73	0.32	-15.8	3.1	
HR 8733	22 57 40.74	+39 18 31.6	217101	6.2	B2IV-V	2.12	0.37	0.19	0.35	-5.42	0.23	-15.5	2.9	
omi And	23 01 55.26	+42 19 33.5	217675	3.6	B6IV/V_sh	4.75	0.53	22.99	0.28	0.88	0.34			
V* LN And	23 02 45.15	+44 03 31.5	217811	6.4	B2V	3.07	0.59	0.35	0.41	-5.82	0.44	-11.3	0.1	
HR 8803	23 07 10.45	+59 43 38.6	218440	6.4	B2V	2.39	0.36	6.70	0.41	-1.68	0.34	-4.6	4.3	
V+ V649 Cas	23 16 27.05	+61 57 46.6	219634	6.5	B0Vn	0.93	0.46	0.33	0.50	-1.85	0.43	-25.8	4.4	
HR 9005	23 46 36.74	+66 46 56.1	223128	5.9	B2IV	2.19	0.27	8.71	0.26	-3.59	0.23	-9.7	0.6	
sig Phe	23 47 16.00	-50 13 35.3	223145	5.2	B3V	5.40	0.25	8.98	0.20	-23.22	0.18	11.0	4.2	
V* V373 Cas	23 55 33.84	+57 24 43.8	224151	6.0	B0.5II-III	0.17	0.32	-3.49	0.33	-0.10	0.24	-24.5	4.3	
HD 224559	23 58 46.44	+46 24 47.4	224559	6.5	B4Vne	2.29	0.43	15.29	0.28	0.19	0.30	-4.0	1.3	2007
sig Cas	23 59 00.54	+55 45 17.7	224572	5.0	B1V	0.72	0.43	8.14	0.34	-5.01	0.32	-12.6	2.8	

Table B.2. Overview over all the measured and calculated parameters. The first three columns give identifier and coordinates and are the same as in Table B.1. The morphological classification we assigned to each nebula (with abbreviations: bow shocks = 'bs', unaligned bow shocks = 'bsna', centered = 'cent', unresolved = 'unres', and not classified nebulae = 'nc'). Columns 5 to 7 indicate whether the star is a known Be star ('Be'), has a nebulous spectrum ('n'), or is a known binary ('bin'). This information is taken from the spectral types in the BSC and the SIMBAD classification, and has to be considered with caution. The distance d and its uncertainties Δd (columns 8, 9) are determined from the parallax. The space velocity is calculated from the radial velocity, proper motion and distance. We determined the total space velocity if the individual uncertainties in distance, proper motion, and radial velocity measurements were $\leq 30\%$. The column 'size_{ang}' contains the angular size of the nebulae and the column 'flux' gives the total flux at 22 μ m. The angular size is converted to physical sizes (column 'size') using the distance d . Column ' α ' displays the misalignment angle α between the proper motion of the star and the bow shock shape (see above). It is only given for bow shocks and unaligned bow shocks. The last two columns give the angular distance $R(0)_{\text{ang}}$ and the physical distance $R(0)$ between the position of the star and the apex of the bow shock.

Ident	RA [J2000]	DEC [J2000]	class	Be	n	bin	d [pc]	Δd [pc]	v_{space} [km s $^{-1}$]	Δv_{space} [km s $^{-1}$]	size _{ang} [' 2 ']	flux [Jy]	size [pc 2]	Δsize [pc 2]	α [$^{\circ}$]	$R(0)_{\text{ang}}$ ['']	$R(0)$ [pc]
HR 38	00 12 50.25	+37 41 37.2	unres				555.56	129.63	0.55	10.03	3.79	0.02	0.014	0.007			
HD 1976	00 24 15.66	+52 01 11.7	bsna		x		306.75	59.28	2.16	25.98	2.55	0.10	0.017	0.007	60	0.7	0.06
HD 2626	00 30 19.93	+59 58 39.2	unres	x	x		235.85	27.81	2.77	25.44	1.26	0.23	0.013	0.003			
lam Cas	00 31 46.36	+54 31 20.2	unres	x	x		115.74	5.76	3.45	27.26	0.68	0.17	0.004	0.001			
kap Cas	00 32 59.99	+62 55 54.4	bs				1369.86	319.01		27.27	6.09				20	3.2	1.28
53 Psc	00 36 47.31	+15 13 54.2	unres				318.47	30.43	1.93	22.20	1.21	0.11	0.017	0.003			
zet Cas	00 36 58.28	+53 53 48.9	bsna				181.82	5.29	36.37	17.24	0.28	0.88	0.102	0.006	80	1.3	0.07
ksi Cas	00 42 04.00	+50 30 45.1	bsna		x		438.6	98.11	67.66	30.80	4.10	3.10	1.101	0.493	25	1.7	0.22
HR 241	00 51 33.79	+51 34 17.1	cent				306.75	33.87	12.94	21.12	2.23	0.71	0.103	0.023			
gam Cas	00 56 42.53	+60 43 00.3	nc	x			187.97	19.79	37.86	23.62	1.08	10.20	0.113	0.024			
HR 287	01 02 18.47	+51 02 05.8	nc				226.24	28.66	1.17	15.49	1.76	0.08	0.005	0.001			
tau And	01 40 34.82	+40 34 37.4	unres				218.34	11.92	2.53	32.76	1.23	0.16	0.010	0.001			
HR 482	01 42 17.70	+58 37 39.9	unres				598.8	193.62	1.19			0.06	0.036	0.023			
phi Per	01 43 39.64	+50 41 19.4	nc	x			220.26	9.7	8.32	29.84	0.54	1.04	0.034	0.003			
1 Per	01 51 59.32	+55 08 50.6	cent				396.83	51.97	29.40	29.02	1.87	3.26	0.392	0.103			
g Per	02 02 18.11	+54 29 15.1	unres				223.21	11.46	1.13	36.58	0.58	0.08	0.005	0.001			
35 Ari	02 43 27.11	+27 42 25.7	unres	x			105.15	9.4	5.41	14.03	9.28	0.39	0.005	0.001			
pi Cet	02 44 07.35	-13 51 31.3	cent		x		120.48	3.05	11.64	15.99	0.38	0.65	0.014	0.001			
HD 18537	03 00 52.21	+52 21 06.2	cent				140.65	22.95	8.33	27.99	1.39	0.80	0.014	0.005			
HD 18538	03 00 53.52	+52 21 07.3	cent				107.64	15.99	8.33	21.56	1.13	0.80	0.008	0.002			
53 Ari	03 07 25.67	+17 52 48.0	unres				255.1	51.41	2.93	37.66	2.23	0.15	0.016	0.007			
55 Ari	03 09 36.74	+29 04 37.5	nc				323.62	51.32	0.85	39.81	2.03	0.07	0.008	0.002			
HR 950	03 12 09.56	+42 22 33.2	nc				200.4	16.06	0.34	25.02	1.02	0.02	0.001	0.001			
HD 20041	03 15 47.97	+57 08 26.2	cent	x			877.19	323.18	53.57			9.15	3.488	2.570			
29 Per	03 18 37.74	+50 13 19.8	unres				195.31	11.06	3.13	30.86	0.56	0.18	0.010	0.001			
HD 20336	03 19 59.27	+65 39 08.3	unres	x	x		233.64	26.2	22.96	20.68	1.33	1.05	0.106	0.024			
HD 21291	03 29 04.13	+59 56 25.2	bsna				595.24	177.15	12.33	8.51	4.60	2.21	0.370	0.220	55	1.7	0.29
HD 21389	03 29 54.74	+58 52 43.5	nc				769.23	331.36									
HR 1092	03 30 51.71	-66 29 23.0	nc				265.96	12.73	1.00	24.48	1.98	0.04	0.006	0.001			
HR 1074	03 32 40.02	+35 27 42.2	bs				675.68	155.22	56.75	40.19	3.86	4.06	2.192	1.007	15	0.7	0.14
o Per	03 42 22.65	+33 57 54.1	cent				323.62	21.99	46.45	24.16	1.47	6.19	0.412	0.056			
del Per	03 42 55.50	+47 47 15.2	bsna	x			158.23	11.77	45.71	37.81	0.77	3.12	0.097	0.014	60	0.8	0.04
17 Tau	03 44 52.54	+24 06 48.0	cent	x			124.07	3.85	37.33	30.50	0.39	18.40	0.049	0.003			
18 Tau	03 45 09.74	+24 50 21.3	nc				125.47	5.82	5.38	30.60	0.39	0.64	0.007	0.001			
20 Tau	03 45 49.61	+24 22 03.9	bs				117.51	3.87	9.81	29.12	0.28	13.41	0.011	0.001	50	0.3	0.01
eta Tau	03 47 29.08	+24 06 18.5	cent	x			123.61	6.42	81.05	28.52	0.46	6.63	0.105	0.011			
HD 23625	03 47 52.67	+33 35 59.5	cent				325.73	87.0	0.70	22.47	2.91	0.03	0.006	0.003			
e Tau	03 48 16.27	+11 08 35.9	bs				139.08	14.7	8.40	30.31	0.81	0.67	0.014	0.003	25	1.3	0.05
27 Tau	03 49 09.74	+24 03 12.3	unres		x		117.23	5.36	11.93	26.47	0.38	0.78	0.014	0.001			
HD 24131	03 51 53.72	+34 21 32.8	unres				258.4	24.04	16.42	22.18	0.91	0.76	0.093	0.017			
31 Tau	03 52 00.23	+06 32 05.7	nc		x		238.66	52.97	2.30	19.31	2.36	0.16	0.011	0.005			
eps Per	03 57 51.23	+40 00 36.8	bs				195.69	8.81	37.72	25.65	0.45	2.32	0.122	0.011	0	3.1	0.18
ksi Per	03 58 57.90	+35 47 27.7	bs	x	x		381.68	74.3	338.08	65.80	1.20	46.06	4.167	1.622	15	10.3	1.14
lam Tau	04 00 40.82	+12 29 25.2	unres		x		148.37	3.74	5.91	17.73	3.03	0.50	0.011	0.001			
35 Eri	04 01 32.05	-01 32 58.8	unres				126.9	4.35	0.51	24.57	0.56	0.03	0.001	0.001			
40 Tau	04 03 44.61	+05 26 08.2	unres				196.46	12.35	2.39	14.14	0.83	0.15	0.008	0.001			

Table B.2. continued.
Article number, page 18 of 21

Ident	RA [J2000]	DEC [J2000]	class	Be	n	bin	d [pc]	Δd [pc]	v_{space} [km s $^{-1}$]	Δv_{space} [km s $^{-1}$]	size _{ang} [' 2 ']	flux [Jy]	size [pc 2]	Δsize [pc 2]	α [']	R(0) _{ang} ['']	R(0) [pc]
lam Per	04 06 35.04	+50 21 04.6	nc	x			129.37	3.68	9.98	24.00	0.72	0.79	0.014	0.001			
41 Tau	04 06 36.41	+27 35 59.6	unres				128.87	5.98	3.22	34.76	0.46	0.24	0.005	0.001			
HR 1307	04 13 34.57	+10 12 44.8	cent		x		132.28	14.17	50.92	22.24	0.89	10.36	0.075	0.016			
mu. Tau	04 15 32.06	+08 53 32.5	cent				139.66	6.63	17.39	25.43	0.52	1.31	0.029	0.003			
HD 27192	04 20 11.51	+50 55 15.4	cent				332.23	41.94	76.69	21.47	2.55	16.96	0.716	0.181			
d Per	04 21 33.17	+46 29 56.0	unres				155.52	6.77	4.23	30.93	0.43	0.33	0.009	0.001			
72 Tau	04 27 17.45	+22 59 46.8	cent		x		115.87	4.57		10.80	1.78						
HR 1415	04 28 32.12	+01 22 51.0	cent				117.37	4.82	6.87	23.78	3.26	0.94	0.008	0.001			
del Cae	04 30 50.10	-44 57 13.5	unres				215.98	8.86	5.39	14.65	0.80	0.12	0.021	0.002			
alf Cam	04 54 03.01	+66 20 33.6	bs				1923.08	702.66	347.72			25.60	108.812	79.516	10	15.2	8.50
HR 1640	05 03 52.12	-14 22 12.8	nc				568.18	132.36	1.33	18.49	4.64	0.05	0.036	0.017			
11 Cam	05 06 08.45	+58 58 20.5	cent	x			210.08	13.68	27.63	15.34	0.80	1.64	0.103	0.013			
105 Tau	05 07 55.44	+21 42 17.4	cent	x			331.13	48.24	12.13	18.68	1.57	1.31	0.113	0.033			
lam Eri	05 09 08.78	-08 45 14.7	bsna	x	x		248.76	11.14	4.49	3.08	2.76	0.28	0.024	0.002	55	2.4	0.17
HD 34078	05 16 18.15	+34 18 44.3	bs				574.71	237.81	124.03			135.06	3.466	2.869	0	0.4	0.07
tau Ori	05 17 36.39	-06 50 39.9	nc				151.52	3.44	4.38	24.66	2.21	0.28	0.009	0.001			
15 Cam	05 19 27.86	+58 07 02.5	unres				240.96	31.35	1.52	21.99	1.79	0.11	0.007	0.002			
HR 1763	05 21 43.56	+08 25 42.8	cent				436.68	68.65		25.95	3.58						
115 Tau	05 27 10.09	+17 57 44.0	unres		x		168.35	9.64	5.28	23.00	0.74	0.37	0.013	0.001			
o Tau	05 27 38.08	+21 56 13.1	cent				191.57	7.71	9.32	17.70	0.25	0.42	0.029	0.002			
ups Ori	05 31 55.86	-07 18 05.5	bsna				877.19	192.37	35.45	26.52	4.33	1.99	2.308	1.012	140	1.9	0.48
HR 1847	05 32 14.14	+17 03 29.2	unres	x	x		917.43	1717.03	4.70			0.82	0.335	1.253			
HR 1861	05 32 41.35	-01 35 30.6	bsna				478.47	183.15	82.47			11.12	1.598	1.223	150	0.2	0.03
VV Ori	05 33 31.45	-01 09 21.9	bsna				450.45	71.02	99.55	4.38	7.77	13.99	1.709	0.539	160	1.3	0.17
120 Tau	05 33 31.63	+18 32 24.8	unres	x			476.19	72.56	12.82	41.48	4.06	1.18	0.246	0.075			
phi01 Ori	05 34 49.24	+09 29 22.5	bsna		x		333.33	27.78	89.32	33.39	9.95	7.51	0.840	0.140	70	4.0	0.39
c Ori	05 35 23.16	-04 50 18.1	cent				271.0	88.13									
121 Tau	05 35 27.13	+24 02 22.5	unres				169.49	6.32	4.48	26.23	0.65	0.38	0.011	0.001			
sig Ori	05 38 44.78	-02 36 00.1	bs		x		328.95	965.2							17	2.0	0.19
ome Ori	05 39 11.14	+04 07 17.3	bsna	x			423.73	52.07	53.40			3.35	0.811	0.199	45	2.5	0.31
125 Tau	05 39 44.20	+25 53 49.5	unres		x		131.06	5.67	4.05	23.12	1.39	0.49	0.006	0.001			
133 Tau	05 47 42.91	+13 53 58.6	unres		x		194.17	13.57	5.39	29.15	0.78	0.50	0.017	0.002			
HR 2058	05 54 34.70	-04 03 53.0	unres				384.62	72.49	8.31	26.46	2.90	0.70	0.104	0.039			
139 Tau	05 57 59.66	+25 57 14.1	bs	x			476.19	43.08	35.82	10.25	3.46	2.67	0.687	0.124	20	2.7	0.37
HD 41335	06 04 13.50	-06 42 32.2	cent	x	x	x	403.23	121.94	38.62			2.57	0.531	0.321			
nu Ori	06 07 34.33	+14 46 06.5	bs		x		158.23	8.26	2.77	28.94	2.28	0.21	0.006	0.001	20	0.7	0.03
del Pic	06 10 17.91	-54 58 07.1	bsna		x		398.41	23.81	29.84	34.90	2.52	0.88	0.401	0.048	50	1.9	0.22
HD 43955	06 18 13.73	-19 58 01.1	unres		x		243.9	16.66	1.79	20.77	2.05	0.11	0.009	0.001			
HR 2276	06 20 52.12	+11 45 22.4	unres				909.09	438.02	3.38			0.15	0.236	0.228			
bet CMa	06 22 41.99	-17 57 21.3	bsna				151.06	5.02	39.46	33.78	0.50	1.62	0.076	0.005	100	5.8	0.25
10 Mon	06 27 57.57	-04 45 43.8	bs				333.33	26.67	6.30	27.28	0.97	0.40	0.059	0.009	10	0.2	0.02
HD 47432	06 38 38.19	+01 36 48.7	bsna				666.67	240.0	61.21			8.23	2.302	1.657	160	2.5	0.48
psi03 Aur	06 38 49.18	+39 54 09.2	nc				420.17	68.85	0.52	30.26	2.64	0.03	0.008	0.003			
HD 48099	06 41 59.23	+06 20 43.5	bsna	x	x		854.7	299.51	51.91			10.02	3.209	2.249	30	4.5	1.12
HD 49662	06 48 57.74	-15 08 41.0	cent				162.07	19.7	8.64	23.37	7.30	1.82	0.019	0.005			
iot CMa	06 56 08.22	-17 03 15.3	bsna				769.23	118.34	1.79	44.09	2.34	0.11	0.090	0.028	25	3.5	0.78
gam CMa	07 03 45.49	-15 37 59.8	unres				135.5	3.86	1.29	32.82	7.22	0.12	0.002	0.001			
V* FN CMa	07 06 40.77	-11 17 38.4	bsna	x			934.58	532.8	12.90			10.90	0.953	1.087	30	2.3	0.63
A Pup	07 08 51.07	-39 39 20.4	unres				223.21	6.98	1.81	23.98	2.29	0.07	0.008	0.001			
HD 54662	07 09 20.25	-10 20 47.6	bs				632.91	180.26	89.48	59.68	3.48	12.12	3.033	1.728	15	6.3	1.16
26 CMa	07 12 12.21	-25 56 33.3	unres				257.07	27.09	0.97	24.58	2.68	0.04	0.005	0.001			
HD 55857	07 13 36.45	-27 21 22.9	bsna				1041.67	455.73	3.68			0.13	0.338	0.296	60	1.1	0.33
HR 2769	07 16 31.85	-38 19 08.1	unres	x			187.27	9.47		33.02	6.98		1.20		0	1.2	
HD 57682	07 22 02.05	-08 58 45.8	bs							12.07							

Table B.2. continued.

Ident	RA [J2000]	DEC [J2000]	class	Be	n	bin	d [pc]	Δd [pc]	v_{space} [km s $^{-1}$]	Δv_{space} [km s $^{-1}$]	size _{ang} [' 2 ']	flux [Jy]	size [pc 2]	Δsize [pc 2]	α ['']	R(0) _{ang} ['']	R(0) [pc]
HR 2812	07 22 13.53	-19 00 59.8	unres				147.49	5.66	12.73	33.27	1.59	0.77	0.023	0.002			
z Pup	07 33 51.04	-36 20 18.2	nc	x	x		363.64	31.74	8.21	17.78	3.90	0.58	0.092	0.016			
e Pup	07 38 43.90	-36 29 48.6	unres				305.81	24.32	4.75	22.72	3.67	0.28	0.038	0.006			
HD 61831	07 39 27.34	-38 18 28.9	nc				170.36	4.64	1.19	33.93	2.19	0.06	0.003	0.001			
HR 3023	07 47 12.55	-22 31 10.2	unres				502.51	83.33	1.09	30.89	2.77	0.05	0.023	0.008			
V* V372 Car	07 52 29.74	-54 22 01.8	bsna				409.84	33.59	4.71	25.17	3.23	0.12	0.067	0.011	80	2.4	0.29
HR 3091	07 54 11.01	-35 52 38.2	unres				207.9	9.94	0.99	28.07	2.77	0.06	0.004	0.000			
V* V Pup	07 58 14.44	-49 14 41.7	bsna		x		294.12	25.09	19.79	20.25	3.34	1.40	0.145	0.025	80	3.0	0.26
HD 66005	07 59 12.31	-49 58 36.8	unres						12.31			0.50					
HD 66006	07 59 13.57	-49 58 25.6	unres						18.47			0.67					
HR 3159	08 00 19.97	-63 34 02.8	unres				153.14	3.05	3.26	26.17	2.37	0.11	0.006	0.001			
HR 3156	08 00 49.94	-54 09 04.6	unres		x		235.29	13.84	0.79	30.00	0.64	0.03	0.004	0.001			
V* V461 Car	08 01 23.04	-54 30 55.9	unres				413.22	42.69	11.77	37.40	6.79	0.35	0.170	0.035			
eps Vol	08 07 55.79	-68 37 01.4	unres		x		172.41	11.59	5.98	34.95	0.62	0.18	0.015	0.002			
16 Pup	08 09 01.64	-19 14 42.1	cent				142.65	4.48	12.18	21.32	1.13	0.90	0.021	0.001			
HD 68895	08 12 30.79	-46 15 51.4	unres		x		320.51	45.2	0.50	19.66	1.95	0.02	0.004	0.001			
V* NO Vel	08 13 36.15	-46 59 29.9	unres		x		416.67	34.72		37.49	3.18						
HD 71510C	08 25 31.10	-51 43 40.0	cent	x			213.22	10.0	2.32	28.84	2.66	0.12	0.009	0.001			
HR 3358	08 29 04.75	-47 55 44.1	nc		x		653.59	145.24	2.69	42.26	4.26	0.09	0.097	0.043			
d Car	08 40 37.03	-59 45 39.6	bsna				442.48	21.54	13.75	22.02	0.77	0.35	0.228	0.022	140	2.9	0.37
eta Hya	08 43 13.47	+03 23 55.2	unres				179.86	7.76	2.47	23.10	0.40	0.13	0.007	0.001			
HR 3479	08 44 51.93	-37 08 50.1	cent				485.44	63.63	19.35	25.06	5.16	2.17	0.386	0.101			
HR 3503	08 48 00.22	-52 51 00.5	nc				141.84	4.83	0.43	25.82	0.73	0.01	0.001	0.001			
f Vel	08 50 33.46	-46 31 45.1	bs		x		1000.0	270.0	99.89	36.06	4.89	11.22	8.452	4.564	0	3.2	0.93
HD 77002	08 56 58.42	-59 13 45.6	unres				206.61	8.96	6.38	29.08	2.59	0.23	0.023	0.002			
E Car	09 05 38.38	-70 32 18.6	bsna	x	x		296.74	33.46	11.42	23.46	6.08	0.67	0.085	0.019	60	1.4	0.12
a Car	09 10 58.09	-58 58 00.8	nc		x		136.99	6.57	5.74	27.47	3.40	0.28	0.009	0.001			
HR 3784	09 30 05.11	-51 31 01.8	unres				132.63	3.52	1.15	17.46	2.41	0.09	0.002	0.001			
zet Cha	09 33 53.38	-80 56 28.5	bs				175.44	4.62	3.62	52.42	3.37	0.15	0.009	0.001	10	1.0	0.05
kap Hya	09 40 18.36	-14 19 56.3	unres				133.69	5.36	1.34	28.70	1.46	0.07	0.002	0.001			
HR 3878	09 45 22.01	-30 12 09.9	bs		x		1075.27	416.23	8.96			0.36	0.877	0.679	0	2.5	0.78
HR 3886	09 46 30.37	-44 45 18.2	unres				305.81	38.34	3.38	19.79	2.14	0.19	0.027	0.007			
HR 3920	09 53 00.09	-55 22 23.5	bs				813.01	178.47	79.13	51.55	5.00	11.41	4.426	1.943	20	0.8	0.19
HD 85980	09 54 17.65	-45 17 00.7	unres				305.81	37.41	3.52	28.25	2.44	0.27	0.028	0.007			
tet Car	10 42 57.40	-64 23 40.0	bs		x		139.66	4.1	43.85	24.73	0.83	7.85	0.072	0.004	15	1.9	0.08
HR 4222	10 46 51.22	-64 23 00.5	unres				147.28	3.69	7.54	21.42	3.14	0.23	0.014	0.001			
HD 96706	11 06 49.89	-70 52 40.5	unres				252.53	14.03	3.48	28.07	1.29	0.09	0.019	0.002			
pi. Cen	11 21 00.44	-54 29 27.9	bsna		x		109.65	4.09	4.24	20.90	1.68	0.16	0.004	0.001	95	2.2	0.07
HD 99104	11 23 21.40	-64 57 17.0	unres				123.76	5.82	4.60	23.78	2.29	0.70	0.006	0.001			
HR 4403	11 24 22.05	-42 40 08.8	unres				847.46	409.37	0.34			0.01	0.021	0.020			
HD 105521	12 08 54.59	-41 13 53.8	nc	x			487.8	59.49	2.04	32.12	1.90	0.16	0.041	0.010			
del Cru	12 15 08.72	-58 44 56.1	cent				105.82	1.68	35.31	29.04	1.99	2.00	0.033	0.001			
G Cen	12 26 31.76	-51 27 02.3	bsna		x		137.36	4.53	32.23	21.63	1.01	0.99	0.051	0.003	120	0.9	0.04
alf Cru	12 26 35.90	-63 05 56.7	bsna		x		98.72	4.87	62.10	21.72	1.35	67.80	0.051	0.005	170	7.4	0.21
sig Cen	12 28 02.38	-50 13 50.3	cent		x		126.26	2.87	5.49	22.27	1.48	0.19	0.007	0.001			
alf Mus	12 37 11.02	-69 08 08.0	bsna		x		96.71	1.03	60.52	23.32	2.23	7.30	0.048	0.001	150	3.1	0.09
bet Mus	12 46 16.80	-68 06 29.2	bsna		x		104.71	4.5	20.03	47.10	6.60	1.93	0.019	0.002	80	0.9	0.03
HD 110956	12 46 22.71	-56 29 19.7	bsna				117.92	3.06	6.53	26.19	1.78	0.54	0.008	0.001	110	1.1	0.04
bet Cru	12 47 43.26	-59 41 19.8	bsna				85.4	7.15	148.89	24.28	0.54	41.09	0.092	0.015	150	5.0	0.12
mu.01 Cru	12 54 35.62	-57 10 40.5	cent				127.06	2.74	10.79	24.45	0.43	0.76	0.015	0.001			
mu.02 Cru	12 54 36.89	-57 10 07.2	cent	x	x		124.84	4.52	23.05	24.60	0.47	1.05	0.030	0.002			
Ksi02 Cen	13 06 54.64	-49 54 22.5	cent		x		143.27	4.93	1.38	24.23	2.43	0.07	0.002	0.001			
HR 5027	13 20 48.34	-55 48 02.5	bs	x			1538.46	1041.42	106.59			9.31	21.347	28.901	15	3.8	1.70
HR 5140	13 42 01.09	-58 47 13.5	unres				239.81	32.78	30.47	39.29	2.11	1.85	0.148	0.041			

Table B.2. continued.

Ident	RA [J2000]	DEC [J2000]	class	Be	n	bin	d [pc]	Δd [pc]	v_{space} [km s $^{-1}$]	Δv_{space} [km s $^{-1}$]	size _{ang} [' 2 ']	flux [Jy]	size [pc 2]	Δsize [pc 2]	α ['']	R(0) _{ang} ['']	R(0) [pc]
nu Cen	13 49 30.28	-41 41 15.8	bsna		x		133.87	3.05	26.08	22.74	0.73	0.96	0.040	0.002	160	2.4	0.09
47 Hya	13 58 31.15	-24 58 20.1	unres	x			102.04	1.98	2.03	28.29	0.75	0.13	0.002	0.001			
eps Aps	14 22 23.16	-80 06 32.2	cent	x			197.63	8.59	35.68	16.75	1.21	2.98	0.118	0.010			
V* HX Lup	14 22 38.71	-48 19 11.5	cent				671.14	261.25	15.17			0.85	0.578	0.450			
tau01 Lup	14 26 08.22	-45 13 17.1	cent				334.45	23.49	43.35	37.89	1.79	4.50	0.410	0.058			
sig Lup	14 32 37.06	-50 27 25.8	bsna		x		176.37	5.91	18.41	27.83	0.35	2.05	0.048	0.003	65	1.4	0.07
bet Lib	15 17 00.41	-09 22 58.5	bsna		x		56.75	0.52	10.40	44.64	1.44	0.64	0.003	0.001	80	0.9	0.01
b Sco	15 50 58.74	-25 45 04.7	bsna				151.75	6.22	14.75	20.99	0.76	1.09	0.029	0.002	35	0.4	0.02
lam Lib	15 53 20.05	-20 10 01.4	unres		x		94.88	8.19	9.73	17.26	1.55	0.94	0.007	0.001			
2 Sco	15 53 36.72	-25 19 37.7	cent	x	x		154.08	12.11	22.33	23.40	0.92	5.77	0.045	0.007			
HR 5906	15 53 53.92	-24 31 59.4	bsna		x		128.87	8.64	6.01	18.49	3.45	0.52	0.008	0.001	80	1.9	0.07
3 Sco	15 54 39.53	-25 14 37.5	bsna				157.98	10.73	0.62	23.23	1.71	0.03	0.001	0.001	80	0.4	0.02
rho Sco	15 56 53.08	-29 12 50.7	bsna		x		144.72	3.98	9.77	20.46	1.63	0.41	0.017	0.001	50	2.2	0.09
48 Lib	15 58 11.37	-14 16 45.7	bsna	x			143.47	4.94	27.67	16.05	0.88	3.54	0.048	0.003	145	2.1	0.09
pi Sco	15 58 51.11	-26 06 50.8	cent		x		179.53	20.63	85.32	25.91	1.13	71.48	0.233	0.053			
del Sco	16 00 20.01	-22 37 18.1	bsna		x		150.6	20.19	139.45	27.00	1.15	36.13	0.268	0.072	45	7.6	0.33
ome Sco	16 06 48.43	-20 40 09.1	bsna				144.51	5.43	38.82	17.79	0.81	3.88	0.069	0.005	70	2.0	0.08
11 Sco	16 07 36.42	-12 44 43.5	nc		x		112.36	7.57	0.63	36.33	5.11	0.05	0.001	0.001			
HR 6026	16 11 58.60	-19 27 00.2	cent						26.78			10.94					
nu Sco	16 11 59.74	-19 27 38.5	bsna		x		145.35	16.06	7.47	17.66	2.50	4.92	0.013	0.003	180	3.0	0.13
13 Sco	16 12 18.20	-27 55 34.9	cent		x		146.84	3.45	33.97	18.57	1.53	6.15	0.062	0.003			
HR 6054	16 14 53.43	-25 28 37.1	cent				148.81	8.86	0.93	18.71	1.31	0.13	0.002	0.001			
sig Sco	16 21 11.32	-25 35 34.1	bsna		x		213.68	27.39	58.22	19.85	1.34	408.94	0.225	0.058	30	2.3	0.14
i Sco	16 30 12.48	-25 06 54.8	cent				126.74	3.86		16.06	0.24						
N Sco	16 31 22.93	-34 42 15.7	cent				170.07	5.5	25.11	17.60	0.31	2.81	0.061	0.004			
tau Sco	16 35 52.96	-28 12 57.7	bs	x	x		145.35	11.2	26.61	17.24	0.66	18.69	0.048	0.007	15	2.9	0.12
zet Oph	16 37 09.54	-10 34 01.5	bs	x	x		112.23	2.52	249.14	17.92	2.77	208.83	0.266	0.012	0	5.9	0.19
HR 6219	16 47 19.66	-58 20 29.2	bs				826.45	211.73	61.59	97.44	5.02	20.54	3.560	1.824	5	1.2	0.29
HR 6387	17 12 25.06	-27 45 43.6	cent	x			153.85	9.47	22.84	35.84	0.61	1.69	0.046	0.006			
V* U Oph	17 16 31.72	+01 12 38.0	unres		x	x	200.4	16.47	1.23	18.90	1.82	0.06	0.004	0.001			
tet Oph	17 22 00.58	-24 59 58.3	cent				133.69	3.04	16.65	16.02	0.51	2.03	0.025	0.001			
HR 6523	17 33 07.39	-41 10 23.0	nc				465.12	90.86	1.74	22.35	3.48	0.08	0.032	0.012			
kap Sco	17 42 29.28	-39 01 47.9	bsna				148.15	3.73	74.44	23.16	1.70	10.77	0.138	0.007	40	3.4	0.15
HD 161056	17 43 47.02	-07 04 46.6	bs				333.33	60.0	29.49	31.68	3.94	3.18	0.277	0.100	5	2.4	0.23
iot02 Sco	17 50 11.11	-40 05 25.6	bsna				781.25	146.48	1.07	19.83	3.78	0.18	0.055	0.021	40	1.3	0.30
HR 6755	18 06 07.40	-08 19 26.2	nc		x		158.73	19.15	2.62	26.32	3.83	0.23	0.006	0.001			
HR 6788	18 10 55.35	-33 48 00.2	bsna						9.50		0.67				75	1.0	
HD 166841	18 18 00.96	-68 13 45.3	unres				186.92	14.67	0.69	24.15	1.52	0.04	0.002	0.001			
HD 170580	18 30 05.12	+04 03 55.3	cent	x			507.61	95.34	1.92	26.98	2.42	0.15	0.042	0.016			
HD 172910	18 44 19.36	-35 38 31.2	bsna				143.06	4.71	9.91	18.90	0.64	0.79	0.017	0.001	45	0.5	0.02
HD 173117	18 44 49.60	-25 00 39.3	cent	x	x		177.3	11.63	13.35	24.20	4.62	1.03	0.036	0.005			
HD 174237	18 46 43.09	+52 59 16.7	unres	x	x		396.83	37.79	2.81	21.13	1.36	0.09	0.037	0.007			
V* V686 CrA	18 56 40.50	-37 20 35.7	bsna				131.93	4.7	72.43	15.88	0.30	4.85	0.107	0.008	80	6.5	0.25
HR 7185	18 59 12.29	+39 13 02.4	unres				292.4	25.65	1.54		0.05	0.011	0.002				
HR 7173	18 59 17.34	+10 08 27.6	bs				662.25	263.15	3.46		0.38	0.128	0.102	0.02	15	1.3	0.25
HR 7202	19 01 17.36	+26 17 29.1	unres				199.2	11.51	1.26	22.21	1.16	0.07	0.004	0.001			
HR 7200	19 01 22.55	+20 49 58.2	nc		x		602.41	141.53	1.69	19.48	4.42	0.07	0.052	0.024			
20 Aql	19 12 40.71	-07 56 22.3	unres				300.3	22.55	1.21	32.72	0.92	0.10	0.009	0.001			
21 Aql	19 13 42.70	+02 17 37.3	nc				217.86	13.76	7.79	8.56	0.64	1.23	0.031	0.004			
1 Vul	19 16 13.04	+21 23 25.5	bsna		x		248.76	22.9	1.66	26.46	9.54	0.17	0.009	0.002	75	1.0	0.07
HR 7361	19 19 46.14	+64 23 26.9	unres				281.69	21.42	1.09	21.66	0.72	0.04	0.007	0.001			
HR 7471	19 38 48.99	+03 22 53.5	nc						0.09			0.01					
sig Aql	19 39 11.64	+05 23 52.0	cent		x		239.23	22.89	29.49	8.00	1.84	4.12	0.143	0.027			
HD 186568	19 43 51.45	+34 09 45.8	nc				331.13	29.6	2.31	15.24	1.04	0.09	0.021	0.004			

Table B.2. continued.

Ident	RA [J2000]	DEC [J2000]	class	Be	n	bin	d [pc]	Δd [pc]	v_{space} [km s $^{-1}$]	Δv_{space} [km s $^{-1}$]	size _{ang} [' 2 ']	flux [Jy]	size [pc 2]	Δsize [pc 2]	α [$^{\circ}$]	R(0) _{ang} ['']	R(0) [pc]
HR 7516	19 45 52.23	-02 53 00.4	nc				362.32	69.58	0.09	17.76	3.07	0.00	0.001	0.001			
9 Sge	19 52 21.76	+18 40 18.8	bsna		x				84.29			2.55			60	7.5	
57 Aql A	19 54 37.65	-08 13 38.2	nc		x		147.93	8.1	0.93	19.60	2.31	0.06	0.002	0.001			
57 Aql B	19 54 38.06	-08 14 13.4	nc				155.76	14.07	0.78	23.33	1.77	0.05	0.002	0.001			
HD 190603	20 04 36.17	+32 13 07.0	cent				1754.39	892.58	81.95			85.92	21.343	21.717			
ome01 Cyg	20 30 03.54	+48 57 05.6	bs				278.55	13.97	14.79	27.71	1.65	4.15	0.097	0.010	10	0.8	0.06
28 Vul	20 38 31.91	+24 06 57.4	unres				160.26	6.16	3.77	24.44	1.13	0.19	0.008	0.001			
ups Pav	20 41 57.08	-66 45 38.4	unres				240.96	15.68	1.79	29.97	1.21	0.16	0.009	0.001			
V* V379 Cep	20 43 13.68	+57 06 50.3	bsna				3225.81	97814.78	18.14			2.59	15.972	968.640	30	1.0	0.94
55 Cyg	20 48 56.29	+46 06 50.9	bsna				714.29	86.73	37.65	15.00	2.53	8.94	1.625	0.395	120	2.6	0.54
BW Vul	20 54 22.40	+28 31 19.2	unres	x	x		320.51	41.09	8.70	10.11	2.32	0.56	0.076	0.019			
HD 199478	20 55 49.80	+47 25 03.6	bsna												65	2.0	
HR 8105	21 11 03.77	+36 17 58.5	bs		x		1149.43	449.2	4.17			0.14	0.466	0.364	10	1.5	0.50
HD 202214	21 11 48.24	+59 59 11.8	bsna				1315.79	727.15	116.80			12.09	17.111	18.912	125	3.5	1.34
HD 203025	21 17 18.79	+58 36 41.3	cent	x			840.34	204.79	108.53	19.42	5.39	26.87	6.485	3.161			
sig Cyg	21 17 24.95	+39 23 40.9	bsna				884.96	148.8	16.50	15.95	3.44	0.71	1.093	0.368	40	1.6	0.41
68 Cyg	21 18 27.19	+43 56 45.4	bs		x	x	1428.57	469.39	165.83			60.45	28.636	18.818	10	3.6	1.50
alf Cep	21 18 34.77	+62 35 08.1	bsna				15.04	0.02	64.27	19.42	0.89	2.62	0.001	0.001	160	5.7	
6 Cep	21 19 22.22	+64 52 18.7	bs	x			609.76	63.21	77.28	27.74	1.82	9.14	2.431	0.504	20	0.6	0.11
HD 207198	21 44 53.28	+62 27 38.0	cent				917.43	202.0	5.35	24.66	4.07	0.13	0.381	0.168			
pi.02 Cyg	21 46 47.61	+49 18 34.5	bsna		x		338.98	39.07	3.60	13.47	6.82	0.16	0.035	0.008	130	2.3	0.23
HR 8341	21 49 26.87	+20 27 44.8	unres				358.42	39.82	2.05	16.42	1.86	0.10	0.022	0.005			
HR 8357	21 52 01.04	+55 47 48.2	unres				460.83	490.56	3.14			0.67	0.056	0.120			
ksi Cep	22 03 47.45	+64 37 40.7	cent		x		29.59	0.93	3.27	34.53	1.28	0.32	0.000	0.001			
lam Cep	22 11 30.58	+59 24 52.2	bs		x		606.06	80.81	177.53	84.36	1.76	52.73	5.518	1.471	0	8.0	1.41
HR 8490	22 13 49.70	+63 09 44.4	nc		x		400.0	40.0		25.90	2.46						
30 Peg	22 20 27.58	+05 47 22.2	nc				390.63	45.78	2.77	39.11	1.62	0.19	0.036	0.008			
4 Lac	22 24 30.99	+49 28 35.0	bs				689.66	166.47	3.66	33.06	3.77	0.23	0.147	0.071	0	1.0	0.20
pi. Aqr	22 25 16.62	+01 22 38.6	bsna	x			239.81	15.53	9.27	21.05	0.70	0.68	0.045	0.006	60	2.0	0.14
HD 212883	22 26 45.56	+37 26 37.3	cent				458.72	130.46	6.04	14.98	3.90	0.52	0.108	0.061			
26 Cep	22 27 05.31	+65 07 56.2	bs	x			1639.34	644.99	159.21			15.37	36.205	28.489	5	5.4	2.58
8 Lac B	22 35 52.11	+39 37 41.3	nc	x			662.25	574.54	6.34			0.55	0.235	0.408			
10 Lac	22 39 15.68	+39 03 01.0	bsna		x		529.1	61.59	69.70	17.04	1.71	3.28	1.651	0.384	135	6.1	0.94
12 Lac	22 41 28.65	+40 13 31.6	bs				411.52	49.11	2.19	16.56	2.16	0.08	0.031	0.007	20	1.6	0.19
HD 215191	22 42 55.48	+37 48 10.1	bsna				321.54	47.56	0.04	19.76	2.89	0.00	0.000	0.001	60	2.3	0.22
HR 8677	22 47 23.24	+58 28 58.9	nc				308.64	36.2		15.55	1.46						
14 Lac	22 50 21.77	+41 57 12.2	nc		x		348.43	55.85	1.71	21.47	2.87	0.08	0.018	0.006			
HR 8733	22 57 40.74	+39 18 31.6	cent				471.7	82.32	3.83	19.69	3.11	0.17	0.072	0.025			
omi And	23 01 55.26	+42 19 33.5	cent	x	x		210.53	23.49	30.13	nan	nan	2.60	0.113	0.025			
V* LN And	23 02 45.15	+44 03 31.5	unres				325.73	62.6	5.73	14.45	1.94	0.30	0.051	0.020			
HR 8803	23 07 10.45	+59 43 38.6	nc		x		418.41	63.02		14.46	2.52						
V+ V649 Cas	23 16 27.05	+61 57 46.6	bsna	x			1075.27	531.85	15.34			4.66	1.501	1.485	120	3.0	0.94
HR 9005	23 46 36.74	+66 46 56.1	bsna				456.62	56.3	10.89	22.60	1.79	0.43	0.192	0.047	80	0.9	0.12
sig Phe	23 47 16.00	-50 13 35.3	unres				185.19	8.57	0.88	24.48	1.93	0.04	0.003	0.001			
V* V373 Cas	23 55 33.84	+57 24 43.8	nc		x		5882.35	11072.66	49.51			1.59	144.960	545.731			
HD 224559	23 58 46.44	+46 24 47.4	nc	x	x		436.68	82.0	1.38	31.93	2.77	0.13	0.022	0.008			
sig Cas	23 59 00.54	+55 45 17.7	bs		x		1388.89	829.48	18.61			0.65	3.038	3.628	20	1.5	0.61